MCST Internal Memo

Date: December 11, 2020
From: Kevin Twedt, Emily Aldoretta, Amit Angal
To: MODIS Science Team Members
Subject: Proposed calibration improvements for the MODIS reflective solar bands in Collection 7 Level 1B processing
Memo #: M1165

---

1. INTRODUCTION

The current algorithms implemented for the MODIS reflective solar bands' (RSBs) look-up-tables (LUTs) in Collection 6.1 (C6.1) utilize both the on-board calibrators (OBCs) along with supplemental Earth-view (EV) data when necessary [1]. The m_1 (1/gain) calibration coefficient is derived using the solar diffuser (SD) calibration measurements and is computed on a band (B), detector (D), sub-frame (SF) and mirror-side (MS) basis:

$$m_1 = \frac{\rho_{SD} \cdot \cos(\theta_{SD})}{dn_{SD}^* \cdot d_{ES}^2} \cdot \Delta_{SD} \cdot \Gamma_{SD} \ ,$$

where ρ_{SD} is the pre-launch SD bidirectional reflectance factor (BRF), θ_{SD} is the solar zenith angle, d_{ES} is the Earth-Sun distance in Astronomical Units (AUs) during the SD calibration, dn_{SD}^* is the digital number of the SD response after instrument temperature and background correction, Δ_{SD} is the on-orbit degradation of the SD plate due to solar exposure, and Γ_{SD} is the SD screen (SDS) vignetting function.

Because the MODIS scan mirror shows a reflectance dependence as a function of the angle of incidence (AOI), the response verses scan angle (RVS), another primary RSB LUT, is calculated by monitoring the relative change in gain from multiple AOIs. The RVS was measured for each band during pre-launch testing. On-orbit, the time-dependent change in RVS is monitored primarily using a combination of SD and lunar data. The final RVS is calculated as [2]:

$$RVS(B, D, MS, \theta, t) = \ RVS_{PL}(B, MS, \theta) \times RVS_{oo}(B, D, MS, \theta, t),$$

where RVS_{PL} is the pre-launch measured RVS, RVS_{oo} is the on-orbit change in RVS (i.e. normalized to 1 at mission start), and θ indicates the AOI dependence. While most RSBs continue to rely on the SD and lunar m_1 (calculated using lunar observations at the Space View AOI via spacecraft roll maneuvers) for this correction, the shorter-wavelength RSBs began to show a drift in their reflectance trends later in the missions at AOIs far from the SV. Supplemental EV data over pseudo-invariant calibration sites (PICS) in North Africa are utilized for Aqua B1-4, 8, 9 and Terra B1-4, 8-10, to calculate the time-dependent EV-based RVS_{oo}. The final RVS LUTs are delivered in the form of a polynomial fit to give the RVS at any AOI [3]:

$$RVS(\theta,t) = c_0(t) + c_1(t)\theta + c_2(t)\theta^2 + c_3(t)\theta^3 + c_4(t)\theta^4.$$

The desert PICS are also used to adjust the m_1 calibration of the same bands to compensate for any inaccuracies in the SD-based calibration. A set of fitted m_1 and RVS forward LUTs are currently generated once a month, usually timed with the collection of new lunar data. The current MCST guidelines for C6.1 [3] dictate that any change in these forward tables greater than 0.2% will trigger a LUT update for all RSBs and their detectors. Out-of-family LUT updates will most likely occur when any instrument behavior caused by a MODIS or spacecraft anomaly is detected within these coefficients.

Several other LUTs are updated on a semi-regular basis for the RSBs in C6.1. These include the time-dependent uncertainty index (UI) [4] which is updated bi-annually, the SWIR out-of-band crosstalk (x_oob_1) which is time-dependent and updated bi-annually for Terra MODIS, the time-dependent quality assessment (QA) LUT, and the time-dependent pre-saturation (dn_sat) LUT.

ALGORITHM IMPROVEMENTS

Several improvements have been discussed, tested, validated and proposed by the MODIS Characterization Support Team (MCST) in preparation for Collection 7 (C7). All the major RSB algorithm improvements for C7 are discussed in this section.

2.1. Polarization correction for bands 3, 8-10 (Terra)

The MODIS instrument on Terra had some modest polarization sensitivity in pre-launch testing [5] and has experienced significant on-orbit changes in the polarization sensitivity, the impact of which is mostly evident at the short wavelengths. In the C6.1 algorithm, the desert data used to derive the RVS are not corrected for polarization effects, and this has led to significant uncertainties in the derived gain for the short wavelength bands (3, 8, 9, and 10), particularly at large scan angles. Previously, the NASA Ocean Biology Processing Group (OBPG) developed a correction to account for the polarization effects on the Terra MODIS L1B [6], [7]. In C7, the OBPG coefficients are used to correct the desert data before its use in the on-orbit RVS estimation. Figure 2.1-1 shows examples of the desert data before and after polarization correction is applied for two different AOIs. For an AOI of 17.8° (near beginning of scan), the polarization correction has little impact, but for an AOI of 59.6° (near end of scan), there is a large difference between the uncorrected and corrected trends, particularly for dates after 2008. Since these data trends are fit as part of the process of generating the m_1 and RVS LUTs, the use of polarization-corrected data results in significant changes in the L1B gains. See ref. [8] for further details.

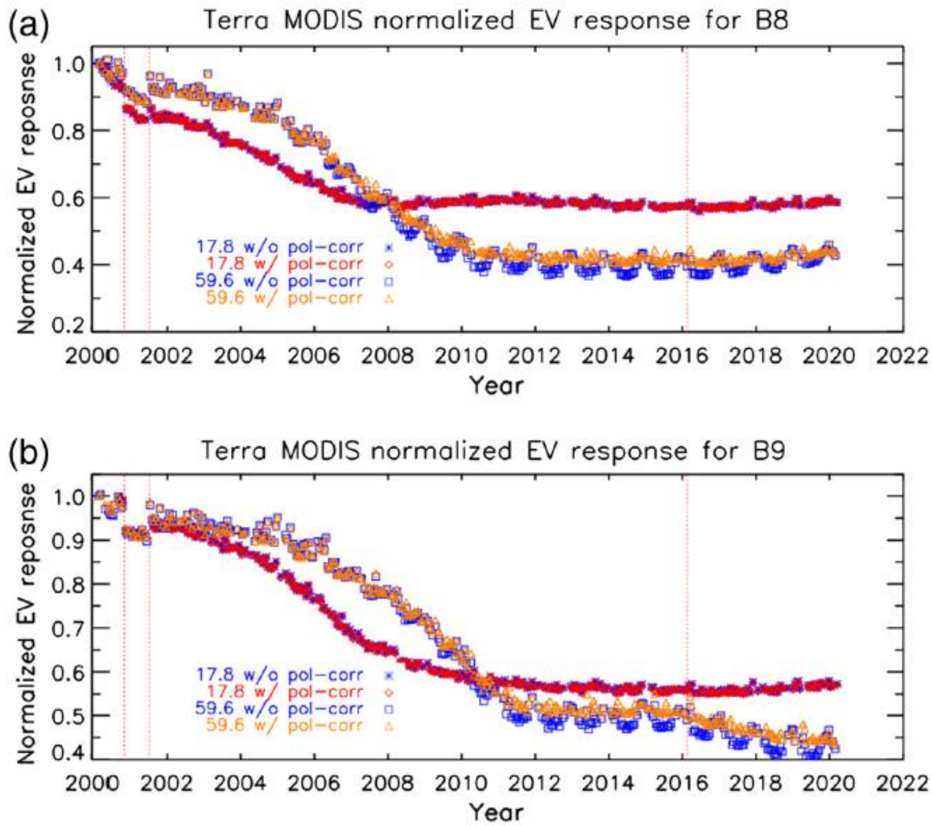

Figure 2.1-1. Earth View response trends from the Libyan desert site for Terra MODIS band 8 (a) and band 9 (b) with and without polarization correction [9].

2.2. SWIR x_oob_1 improvements (Terra)

The Terra MODIS SWIR bands have a known issue related to a 5.3-µm out-of-band (OOB) thermal leak, along with an electronic crosstalk, that was identified prelaunch. The crosstalk correction algorithm implemented in the MODIS L1B calibration process since launch utilizes the regularly scheduled night-time-day-mode observations to derive the crosstalk coefficients that are used to correct the gains (from SD) as well as the uncalibrated EV response. Based on early observations from the MODIS Airborne Simulator field campaigns, band 28 (7.325 µm) was chosen as a surrogate sending band for Terra MODIS to simulate the OOB radiances as MODIS does not have a spectral band centered at 5.3 µm.

In recent years, the Terra MODIS photovoltaic (PV) long-wave infrared (LWIR) bands' (27 to 30) electronic crosstalk has increased considerably, especially following the spacecraft safe-mode event in February 2016 [10]. This accentuated degradation in the PV LWIR performance has also impacted the performance of the SWIR crosstalk correction and thus its calibration and data quality. The use of band 25 as a sending band, also employed in Aqua MODIS, has shown to largely mitigate these artifacts and has resulted in an improvement of the on-orbit gain stability for the SWIR calibration, along with reducing detector-to-detector and subframe-to-subframe striping in the calibrated imagery [11]. In the case of Aqua MODIS, where the artifacts due to crosstalk are significantly smaller, band 25 (4.52 μm) is currently used as a sending band and, based on the excellent on-orbit performance, no change is proposed for C7.

2.3. Time-dependent RVS for the Terra SWIR bands

As stated above, band 25 will be used as the reference band for the Terra MODIS SWIR crosstalk correction for the entire mission in Collection 7 LUTs. After making this change, the solar diffuser calibration is evaluated in the same manner as before, and the measured SD-derived m_1 values are fitted to piecewise polynomial functions of time to get the initial m_1 LUTs. For the SWIR bands in all previous MODIS Collections, the pre-launch RVS LUTs have been used for the entire mission, with no on-orbit correction to the RVS. For Collection 7, we introduce an Earth-based calibration for the SWIR bands (similar to that currently in use in C6/C6.1 for select shorter-wavelength bands) to derive a time-dependent RVS and a time-dependent correction to the SD m_1 values. A time-dependent RVS will be applied for bands 5 and 26, which show up to 2% change in RVS on-orbit, while bands 6 and 7 continue to show stable RVS and will continue to use pre-launch RVS in C7.

We primarily use deep convective clouds (DCCs) as a stable reference for evaluating the reflectance product performance for all SWIR bands: 5, 6, 7, and 26 [12], [13]. We also use the PICS from the Libyan desert to evaluate the performance of bands 5, 6, and 7 (the desert observations do not provide useful data for band 26). Both targets show consistent trends that agree well with each other. For C7 calibration, the reflectance of these Earth targets is first calculated for each band and mirror side (averaged over all detectors and sub-frames) using the SD m_1 and the pre-launch RVS LUTs. Note that lunar observations are not used to derive on-orbit RVS for the SWIR bands due to complications with the crosstalk correction [14]. The resulting reflectance trends are fit over time and frame (AOI) to derive the on-orbit gain change; an example is shown in Fig. 2.3-1. These fits are used to derive the on-orbit RVS LUTs and to apply corrections on top of the SD m_1 LUTs, effectively forcing the C7 calibration to produce flat reflectance trends when evaluated with the same DCC and desert targets. Bands 5 and 26 show a gradually increasing RVS on-orbit, with the end-to-end on-orbit RVS changing up to 2.5% by year 2020. Bands 6 and 7 do not show any significant change in RVS and thus continue to use the pre-launch RVS. The EV-based correction to m_1 LUTs is applied to all four SWIR bands.

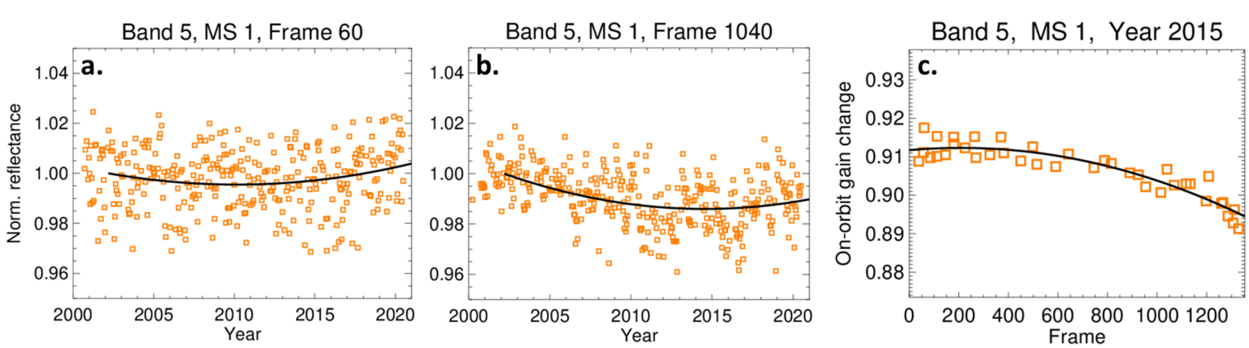

Figure 2.3-1. Normalized reflectance trends from Libya 4 desert site using SD m_1 and pre-launch RVS for Terra band 5 mirror side 1 (a) frame 60 (near beginning of scan) and (b) frame 1040 (near SD AOI). Orange points are individual site observations and black lines are quadratic fits. (c) On-orbit gain change as a function of frame for Terra band 5 mirror side 1 in year 2015, from combining the results of observations of multiple viewing angles of Libya 1, Libya 2, and Libya 4 sites.

For Aqua MODIS, SWIR bands in C7 will continue to use band 25 as the reference band for crosstalk correction, SD-based m_1, and pre-launch RVS, as was done in C6/C6.1. DCC and desert reflectance trends have been studied and they continue to show stable performance of this calibration with no on-orbit change in RVS. Therefore, no EV-based calibration corrections will be used for Aqua SWIR bands.

2.4. Interband calibration for Terra bands 11 and 12

The degradation of the solar diffuser, together with the lack of OBCs to cover additional scan angles other than the one for the lunar observations, has resulted in the use of Earth view responses from the PICS to track the on-orbit RVS changes [2]. This approach has been implemented in C6 and C6.1 for bands 1-4, 8 and 9 of both instruments and additionally for band 10 of Terra MODIS. As the missions continue to operate over a decade beyond their designed lifetimes, and the instrument optics continue to degrade, it is expected that the OBC-based RVS currently applied to other bands, specifically the high-gain ocean bands, will be inadequate to maintain the long-term calibration stability. An interband calibration approach has been formulated and will be implemented in C7. The proposed approach relies on the use of a spectrally-matching stable reference band to evaluate the long-term calibration stability of the high-gain ocean bands that typically saturate while viewing the desert PICS. Ocean reflectance trends are constructed using a ratio of the target ocean band (e.g. band 12) with a reference band (e.g. band 4), and the assumption that the calibration of the reference band is accurate. Results from this approach indicate a noticeable reflectance drift for Terra MODIS bands 11 and 12 using the C6/C6.1 calibration (based on SD and lunar data for these bands), whereas the Aqua bands continue to show excellent temporal stability [15]. In C7, the ocean reflectance trends from the interband calibration approach will be fit in time and AOI to derive a correction to both the m_1 and RVS LUTs. This correction will be applied only to Terra bands 11 and 12, with an impact of up to about 3% (see Section 3).

2.5. Aqua VF improvements

The MODIS high-gain ocean color bands (8-16) are calibrated with the SDS closed to avoid saturation. Therefore, the characterization of the vignetting function (VF) of the SDS is necessary for calibrating the detector gain coefficients of these bands. Due to the lack of pre-launch characterization, a series of yaw maneuvers were carried out on-orbit for both Terra and Aqua to enable its characterization early in their missions. The VF currently used in C6 and C6.1 was derived from the yaw data of low-gain bands 3, 4, 18, and 19, and is applied to the high-gain ocean color bands with the assumption that all spectral bands should have the same VF. Any VF error introduced by this method has been carried over into the gain coefficients calibrated with the SDS closed for these high-gain bands. More recently, a different approach was used to derive the VF from the yaw maneuver data that takes into account the frame-level mismatch between different detectors' footprints on the SD. A set of band- and detector-dependent VFs of all bands are derived from the VF of any reference low-gain band by applying proper SD image frame adjustments [16], [17]. The implementation of this new VF into the C7 calibration of the ocean color bands effectively reduces the undesired detector-dependent seasonal oscillation observed in the long-term trending of their gain coefficients. Figure 2.5-1 shows the ratio between the m_1 values of select Aqua high-gain bands before (C6.1) and after (C7) the implementation of the new, detector-dependent VF. The reduction in the seasonal oscillations of the gain trends allows for more accurate short-term tracking of gain changes and more accurate forward prediction but does not significantly change the long-term (multi-year) gain trends.

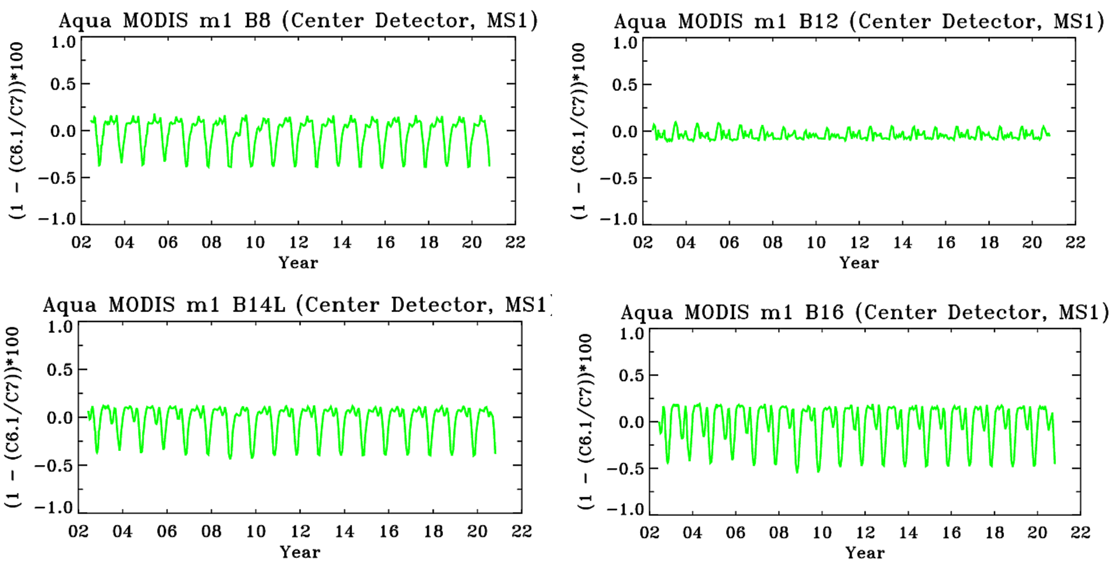

Figure 2.5-1. Percent differences of the entire-mission reprocessed SD m_1 between C6.1 and C7 for B8 (*upper left*), B12 (*upper right*), B14 (*lower left*) and B16 (*lower right*) mirror side 1 center detector.

2.6. Fitting improvements to EV-based calibration (Extra frames, AOI first vs. time first, time-fitting using smoothing window approach)

Within the current C6/C6.1 algorithm, EV PICS are used for certain RSBs to compensate for drifts seen in reflectance at AOIs far from the SD and SV AOIs [2]. For Aqua MODIS, these bands include B1-4, 8, and 9 while Terra utilizes this EV-based RVS approach for B1-4, 8-10. While this EV-based RVS approach has shown significant improvement over utilizing the OBCs alone, several tests have been performed within MCST to continue to enhance this RVS approach and will be incorporated within C7.

The first improvement being made for the C7 EV-based RVS approach is the use of extra frames from the PICS. Currently in C6/C6.1, only a handful of the available frames are used, which were carefully selected during the initial C6 tests. Over time, the use of more frames has been found to improve the current AOI fitting for each band/mirror side that utilizes the EV-based RVS approach. The C6/C6.1 frames, along with the additional C7 frames, are listed in Figures 2.6-1 and 2.6-2 for Aqua and Terra, respectively.

Aqua EV frames	
Site	Frame numbers
C6 (original)	43, 106, 150, 228, 326, 445, 501, 650, 731, 800, 939, 1056, 1205, 1313
Algeria 3	42, 89, 148, 223, 319, 435, 570, 713, 850, 979, 1083, 1232, 1285, 1325
Libya 1	39, 88, **150**, 231, 334, 460, 606, 758, 902, 1026, 1127, **1205**, 1266, **1313**
Libya 2	53, **106**, 173, 260, 369, **501**, **650**, **800**, **939**, **1056**, 1149, 1222, 1279, 1323
Libya 4	**43**, 90, **150**, **228**, **326**, **445**, 584, **731**, 873, 997, 1099, 1181, 1245, 1295, 1333

grey = unused, black = new frame, **bold** = frame that was also an original frame

Figure 2.6-1. List of additional frames used for the EV-based RVS bands for Aqua C7.

Terra Bands 1-4, 8-9 EV frames	
Site	Frame numbers
C6 (original)	38, 111, 146, 225, 325, 450, 591, 642, 745, 890, 1040, 1134, 1329
Algeria 3	44, 91, 151, 227, 322, 439, 574, 719, 860, 983, 1085, 1170, 1285
Libya 1	57, **111**, 180, 269, 381, 515, 666, 815, 954, 1069, 1286, **1329**
Libya 2	**38**, 85, **146**, **225**, **325**, **450**, **591**, **745**, **890**, 1015, 1117, 1198, 1260, 1307
Libya 4	21, 60, 112, 179, 264, 370, 498, **642**, 788, 924, **1040**, **1134**, 1208, 1266, 1312

grey = unused, black = new frame, **bold** = frame that was also an original frame

(a)

Terra Band 10 (t < 3000) EV frames	
Site	Frame numbers
C6 (original)	322, 439, 574, 719, 860, 983, 1085, 1170
Algeria 3	44, 91, 151, 227, **322**, **439**, **574**, **719**, **860**, **983**, **1085**, **1170**, 1285
Libya 1	57, 111, 180, 269, 381, 515, 666, 815, 954, 1069, 1286, 1329
Libya 2	38, 85, 146, 225, 325, 450, 591, 745, 890, 1015, 1117, 1198, 1260, 1307
Libya 4	21, 60, 112, 179, 264, 370, 498, 642, 788, 924, 1040, 1134, 1208, 1266, 1312

Terra Band 10 (t > 3000) EV frames	
Site	Frame numbers
C6 (original)	44, 91, 111, 180, 269, 381, 439, 515, 642, 745, 890, 983, 1134
Algeria 3	**44**, **91**, 151, 227, 322, **439**, 574, 719, 860, **983**, 1085, 1170, 1285
Libya 1	57, **111**, **180**, **269**, **381**, **515**, 666, 815, 954, 1069, 1286, 1329
Libya 2	38, 85, 146, 225, 325, 450, 591, **745**, **890**, 1015, 1117, 1198
Libya 4	21, 60, 112, 179, 264, 370, 498, **642**, 788, 924, 1040, **1134**, 1208, 1266, 1312

grey = unused, black = new frame, **bold** = frame that was also an original frame

(b)

Figure 2.6-2. List of additional frames used for the EV-based RVS for (a) bands 1-4, 8, 9 and (b) band 10 for Terra C7.

The current EV-based RVS technique [2] that is implemented in C6/C6.1 first fits the desert data (the EV dn after correcting for instrument background, temperature, and site BRDF) over time at each of the frames listed in Figures 2.6-1 and 2.6-2. This fitted curves at each frame are then combined and a fit over AOI is performed at a series of times, giving the on-orbit RVS change as a smooth function of AOI and time over the mission. This method relies upon the 16-day repeatability of the data at each of the desert PICS at the specified frames used in the current collection. However, at some point in both missions, the satellites will be taken out of their current orbit and allowed to drift. This 16-day repeatability will no longer be reliable as both MODIS instruments will view these desert PICS at other frames during this period. To prepare for this, C7 will begin implementing a technique in which the PICS data are binned each month, fitted with respect to AOI first, and then fitted with respect to time (normalized to mission start). Figure 2.6-3 shows an example of the initial, monthly-binned AOI fit for the Libya 1, 2, and 4 PICS separately. After each site is treated independently, the fitted EV-dn data are then combined and fitted with respect to time. The final, combined AOI fit to determine the RVS is shown in Figure 2.6-4. While this simple fitting change was made in preparation for the constellation exit, more work will still be required to improve the BRDF correction and/or atmospheric corrections used for these desert PICS in order to continue using this calibration algorithm during orbit drifting.

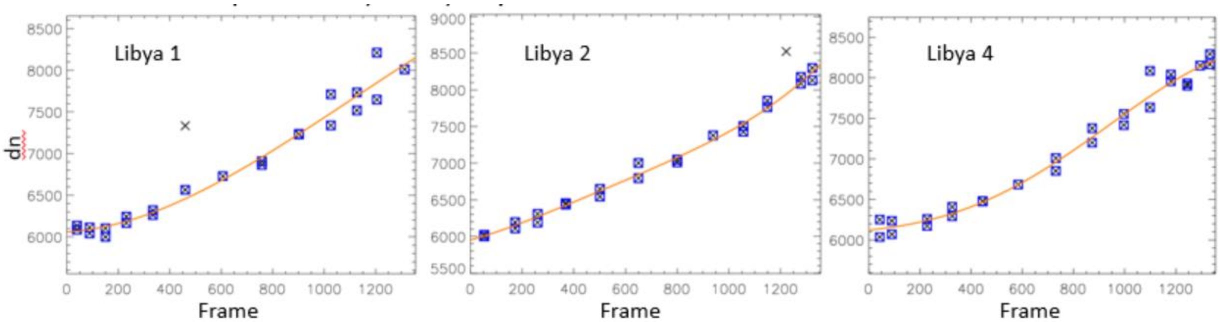

Figure 2.6-3. Initial, monthly-binned AOI fit of the Libya PICS for Aqua B8 MS1 of July 2012. Data outliers marked by “x” are not included in the fit.

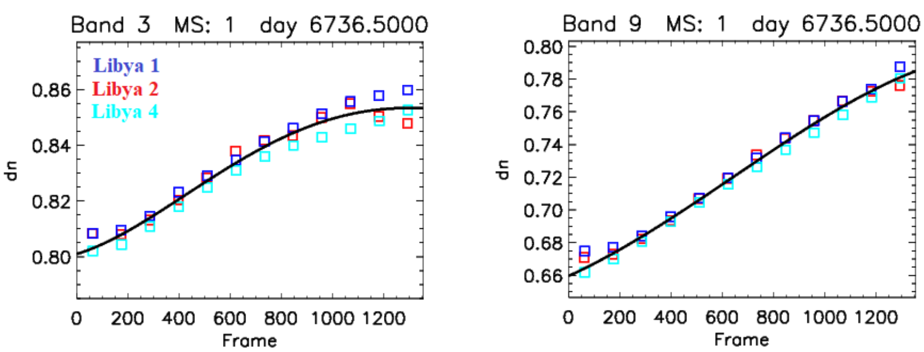

Figure 2.6-4. Final, combined AOI fit to determine the *RVS* for Aqua B3 (*left*) and B9 (*right*) MS1 for a date in year 2020.

The last algorithm enhancement to the EV-based RVS within C7 is the use of a sliding-window average within the EV-dn time fitting. Currently in C6/C6.1, this fitting method utilizes piecewise fitting segments in order to fit the desert reflectance over time. However, due to the variability within the data and the inadequacy of the piecewise method, a 2-year sliding average method shows some improvement within the fitting residuals.

2.7. Extend D2D RVS for Terra band 4

The on-orbit change in RVS for most bands is defined separately for each band and mirror side, but all detectors within a band have the same RVS values. In Collection 6/6.1, a handful of bands are an exception to this, and use a detector-dependent RVS function: Terra bands 3, 8-12 and Aqua bands 8-12 [2]. In addition to these bands, Terra band 4 will also use detector-dependent RVS in Collection 7. The same algorithm for detector-dependent RVS will be used in C7 as is currently used in C6/C6.1. The detector differences from the lunar observations and the SD observations are combined to derive a two-point RVS function at the detector level. We recently used detector differences observed in DCC reflectance to evaluate the calibration performance for Terra and Aqua bands 1, 3, and 4 [18]. Terra band 4 was found to show improved stability and reduced striping in the DCC reflectance product when the detector-dependent RVS algorithm is applied. For Aqua bands 3 and 4, the current band-average RVS algorithm continues to give excellent performance in the DCC trends, so there is no need for a detector-dependent RVS correction.

2.8. Re-processed LUTs generated using consistent algorithms

The C6 L1B product, which began production in 2012, included several improvements to the RSB LUTs [2]. One such improvement was the use of EV PICS for the RSB characterization of the shorter wavelength bands (1-4, 8, 9). Over the course of C6 however, band 10, calibrated using the OBC-based RVS alone, began showing drifts in its reflectance. Therefore, starting in May 2014, the MCST initiated the use of EV PICS for this band as well within C6 forward production. While Terra bands 1-4, 8 and 9 utilize the Libya 1, 2, and 4 PICS for their EV-based RVS characterization, Terra band 10 exhibits saturation at these PICS before March 2008. Therefore, Terra band 10 utilizes the Algeria 3 PICS within the EV-based RVS before this time, with the Libya PICS used after this time. For the C7 product, Terra band 10, along with the other short wavelength bands, will be reprocessed from the start of the mission utilizing the EV-based RVS approach. Also note that the desert data used for Terra band 10 in C7 will be corrected for polarization (see Section 2.1).

More generally, all calibration LUTs are regenerated for C7 using consistent algorithms and fitting strategies over the entire MODIS missions. This will improve the quality of the LUTs and reduce noise and errors associated with the inaccuracies of forward prediction which exist in the C6 LUTs from the start of production in 2012 through the current date. Lastly, we note that a slightly different lunar calibration method is used to derive the C7 RVS LUTs. The C7 lunar calibration will use only scans which view the full disk of the Moon, as opposed to the current approach in C6 that generates images of the Moon for each detector by combining the results of all scans with a partial view of the Moon [19]. The change results in a slightly smoother long-term trend of the lunar results, particularly for the mirror-side ratio, but does not have a significant impact on the long-term RVS calibration.

3. IMPACT ASSESSMENT AND COMPARISONS WITH C6.1

In this Section, we review the impact on the L1B reflectance and radiance products of the RSB algorithm changes discussed in Section 2. In general, the overall impacts of the changes are most significant for the Terra MODIS short-wavelength bands 3, 8-12, and SWIR bands. For other Terra MODIS RSB and for all Aqua MODIS RSB, the overall differences in gain and reflectance between C6.1 and C7 are generally within 1% and there are no major impacts expected on the downstream products. Appendix A at the end of this document contains a full set of plots showing the percent difference in the m_1/RVS (inverse gain) between the C6.1 LUTs and the planned C7 LUTs for each RSB of both Terra and Aqua MODIS.

By far the most significant impact on the calibrated gains and thus the L1B reflectance comes from the use of polarization-corrected desert data in deriving the RVS for Terra bands 3, 8, 9, and 10. Figure 3-1 shows the impact of the polarization correction on the instrument gain at three different AOIs for bands 3, 8, and 9. For AOIs near the beginning of scan (11.25°) and at nadir (38.25°), the impact is relatively minor. However, near the end of scan (60°), the impact is more than 15% at certain times of the mission for band 8.

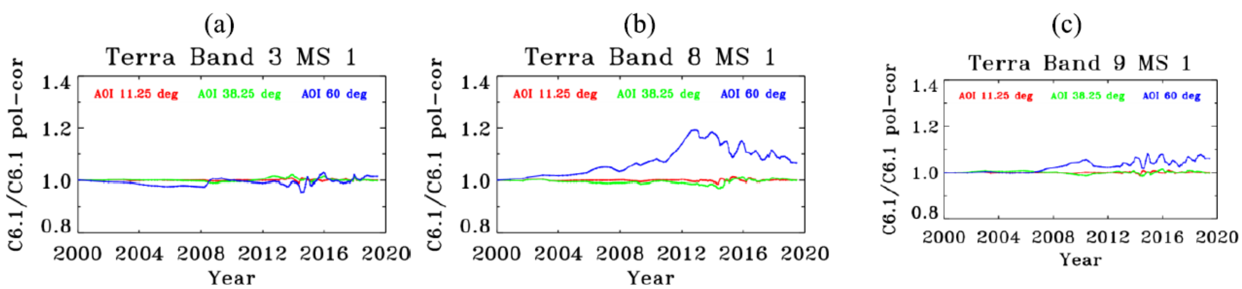

Figure 3-1. Ratio between the C6.1 gain and the reprocessed gain using polarization-corrected desert data for Terra (a) band 3, (b) band 8, and (c) band 9 at select AOI [8]. Curves are shown at AOI of 11.25° (red), 38.25° (green), and 60° (blue).

The plots in Fig. 3-1 show the impact of using polarization-corrected desert data on the calibrated gains, and by extension the L1B reflectance. It is important to note, though, that there is no polarization correction applied to the L1B data itself, since this would be a scene-dependent correction. Also, the impact on downstream science products will not be this significant, since there are already polarization mitigation strategies in place in C6.1. The primary goal and impact of this change is to improve the accuracy of the L1B reflectance and reduce the magnitude of the downstream corrections that need to be applied on top of the L1B reflectance.

The changes made to the Terra SWIR bands, to improve the crosstalk correction (using band 25 as the reference band) and to introduce an on-orbit RVS for bands 5 and 26, also result in a relatively significant change in the reflectance in C7 relative to C6.1. The main impact of the crosstalk sending band switch is a dramatic improvement in the sub-frame (along-scan) and detector (along-track) striping for dates after the February 2016 safe hold event. Figures 3-2 and 3-3 show example image histograms from individual granules in 2010 and 2019, respectively.

Both the C6.1 case (band 28 sending band) and the C7 case (band 25 sending band) are shown. In 2010 (Fig. 3-2), there is little difference between the C6.1 and C7 cases, but in 2019 (Fig. 3-3), there is a significant reduction in striping for C7, seen as a tighter spread of the curves for individual detectors.

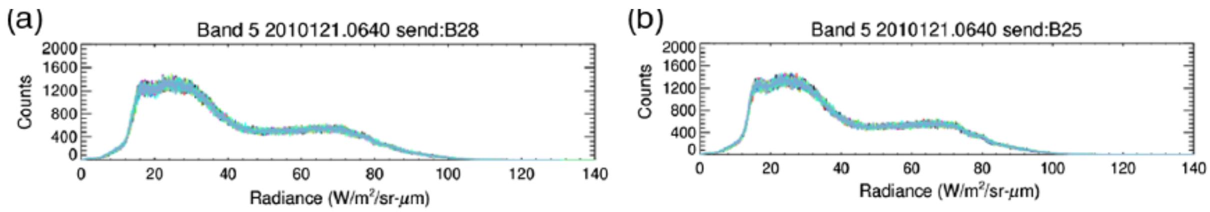

Figure 3-2. Earth view radiance histograms for Terra band 5 using (a) C6.1 band-28 based and (b) C7 band 25-based calibration for 2010121.0640 granule [11].

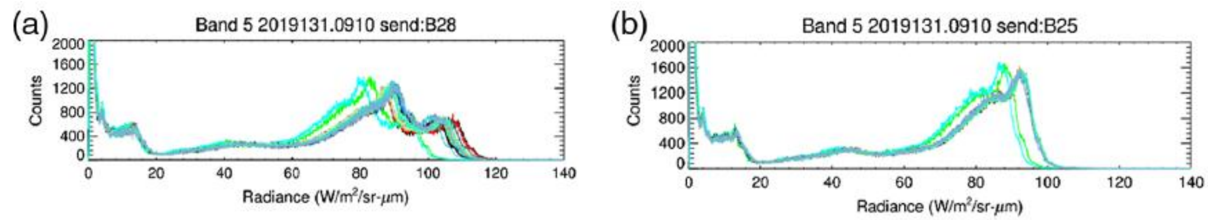

Figure 3-3. Earth view radiance histograms for Terra band 5 using (a) C6.1 band-28 based and (b) C7 band 25-based calibration for 2019131.0910 granule [11]. Note that detectors 3 and 5, which appear as outliers in both versions, are flagged as having out-of-family gain in the L1B since 2017, due to reasons unrelated to the crosstalk correction.

The C7 Terra SWIR band-averaged (averaged over all detectors and subframes) gain at the SD AOI is not significantly different from C6.1, with differences within ±1% (see Appendix A) for dates through 2015. For dates after the February 2016 safe mode event, the previous C6.1 calibration using band 28 had significant errors, so a larger difference up to a few percent is seen between C6.1 and C7 in this time period. Also, for bands 5 and 26, the inclusion of on-orbit RVS results in gain differences at other AOIs of up to 2% between C6.1 and C7, with the difference growing gradually over the mission. Overall, the C7 reflectance trends, as evaluated using DCC and desert sites, will be more stable across all AOIs than in C6.1.

The interband calibration used for Terra bands 11 and 12 results in calibration differences of up to about 2%. Figure 3-4 shows the normalized reflectance over ocean scenes derived using interband calibration for Terra bands 11 and 12, using band 4 as the spectrally-matched reference band. The reflectance here is calculated using the OBC-based (lunar and SD data only) calibration, which was the calibration methodology for C6/C6.1, and curves are shown at three different AOIs. While the lunar AOI shows relatively flat trending, a deviation of up to 3% is seen for band 11 at nadir and SD AOIs. These trends are fit in time and AOI in order to derive the new calibration for C7. The final comparisons of C6.1 to C7 calibrated gains for these bands are shown in Appendix A.

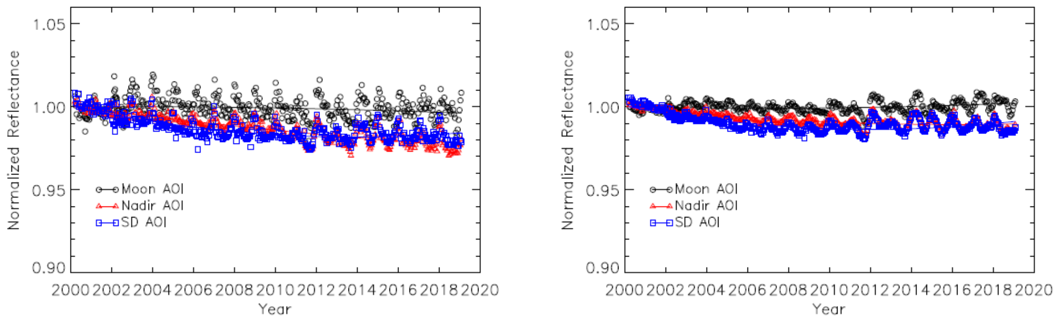

Figure 3-4. Normalized reflectance of Terra MODIS band 11 (left) and band 12 (right) over ocean scenes using an interband calibration approach and band 4 as a reference band [15].

The other calibration improvements discussed in Section 2 have comparably smaller impacts on the calibrated gains. The VF improvements for Aqua and the fitting enhancements applied to the desert data for both instruments allow for more accurate tracking of the gain over short time periods within the mission. They will also lead to more accurate gain prediction once C7 LUTs are being generated in forward production, but they do not lead to any significant change in the multi-year trends. The changes manifest as short-term fluctuations in the m_1/RVS comparison plots in Appendix A, generally within ±1% in most cases, though they can be larger for some bands (Terra band 8) and for AOIs near the very edge of scan. One notable improvement for C7, resulting from the combination of the use of polarization-corrected data and the RVS fitting enhancements, is a reduction in the mirror side striping in L1B reflectance for Terra bands 3, 8, and 9. In C6.1 L1B, for certain times in the mission, there were noticeable mirror side differences in the reflectance of up to a few percent. These arose from calibration errors in the fitting of the desert data (uncorrected for polarization). Figure 3-5 shows a comparison of the mirror side reflectance ratio for C6.1 vs C7 for Terra band 8 observations from the Libya 4 desert site. Our new approach for C7 effectively eliminates the mirror side striping.

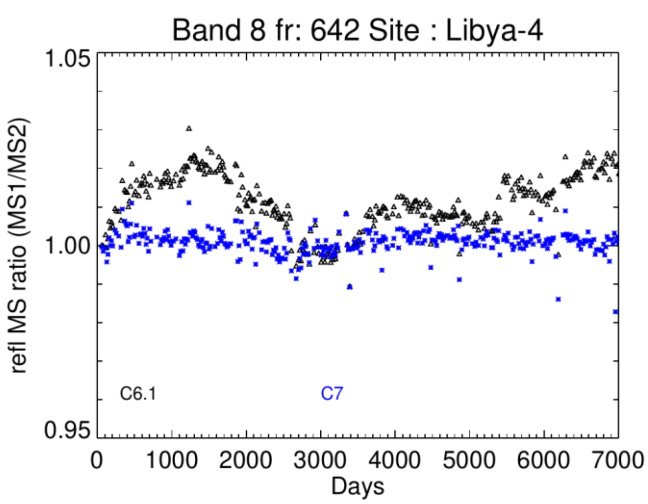

Figure 3-5. Ratio of reflectance from mirror side 1 to mirror side 2 from observations of Libya 4 desert site using C6.1 (black) and C7 (blue) calibration algorithm for Terra band 8 near nadir. For

both curves in this plot, the Libya 4 dn are corrected to remove polarization impact, and the only difference is the m_1/RVS LUTs used to evaluate the reflectance.

4. SUMMARY

We have reviewed the RSB algorithm changes that are planned to be implemented in Collection 7 L1B LUTs, relative to the algorithms used for the Collection 6.1 L1B LUTs. The majority of the discussed algorithm changes apply only to Terra MODIS, with relatively large changes of several percent seen for the short wavelength bands 3, 8-12, and SWIR bands. Aqua MODIS largely retains the C6.1 calibration strategies and there will be relatively small (<1% in nearly all cases) differences between the C6.1 and C7 L1B products. Overall, the C7 RSB reflectance and radiance products will provide a more accurate and stable calibration over the entire MODIS missions. While this memo documents the final calibration algorithms that will be used to deliver the initial C7 calibration LUTs, MCST will continue to work to maintain and improve MODIS RSB calibration going forward. Importantly, several different strategies are currently being explored to enable calibration of the MODIS instruments after the constellation exit maneuvers and extend the useful lifetime of MODIS data as far into the future as possible.

References

[1] X. Xiong *et al.*, “MODIS Reflective Solar Bands On-Orbit Calibration and Performance,” *IEEE Trans. Geosci. Remote Sens.*, vol. 57, no. 9, pp. 6355–6371, 2019, doi: 10.1109/TGRS.2019.2905792.

[2] J. Sun, X. Xiong, A. Angal, H. Chen, A. Wu, and X. Geng, “Time-Dependent Response Versus Scan Angle for MODIS Reflective Solar Bands,” *IEEE Trans. Geosci. Remote Sens.*, vol. 52, no. 6, pp. 3159–3174, Jun. 2014, doi: 10.1109/TGRS.2013.2271448.

[3] E. J. Aldoretta *et al.*, “The MODIS RSB calibration and look-up table delivery process for collections 6 and 6.1,” in *Proceedings of SPIE*, Aug. 2020, vol. 11501, p. 115011Q, doi: 10.1117/12.2570785.

[4] X. Xiong *et al.*, “Updates of Moderate Resolution Imaging Spectroradiometer on-orbit calibration uncertainty assessments,” *J. Appl. Remote Sens.*, vol. 12, no. 03, p. 1, Jul. 2018, doi: 10.1117/1.JRS.12.034001.

[5] Jun-Qiang Sun and Xiaoxiong Xiong, “MODIS Polarization-Sensitivity Analysis,” *IEEE Trans. Geosci. Remote Sens.*, vol. 45, no. 9, pp. 2875–2885, Sep. 2007, doi: 10.1109/TGRS.2007.900672.

[6] E. J. Kwiatkowska, B. A. Franz, G. Meister, C. R. McClain, and X. Xiong, “Cross calibration of ocean-color bands from Moderate Resolution Imaging Spectroradiometer on Terra platform,” *Appl. Opt.*, vol. 47, no. 36, p. 6796, Dec. 2008, doi: 10.1364/AO.47.006796.

[7] G. Meister, R. E. Eplee, and B. A. Franz, “Corrections to MODIS Terra calibration and polarization trending derived from ocean color products,” in *Proceedings of SPIE*, Oct. 2014, vol. 9218, p. 92180V, doi: 10.1117/12.2062714.

[8] A. Angal *et al.*, “On-Orbit Calibration of Terra MODIS VIS Bands Using Polarization-Corrected Desert Observations,” *IEEE Trans. Geosci. Remote Sens.*, vol. 58, no. 8, pp. 5428–5439, Aug. 2020, doi: 10.1109/TGRS.2020.2966000.

[9] X. Xiong *et al.*, “Terra MODIS: 20 years of on-orbit calibration and performance,” *J. Appl. Remote Sens.*, vol. 14, no. 03, p. 037501, Aug. 2020, doi: 10.1117/1.JRS.14.037501.
[10] T. Wilson *et al.*, “Development and Implementation of an Electronic Crosstalk Correction for Bands 27–30 in Terra MODIS Collection 6,” *Remote Sens.*, vol. 9, no. 6, p. 569, Jun. 2017, doi: 10.3390/rs9060569.
[11] X. Xiong, A. Angal, Y. Li, and K. Twedt, “Improvements of on-orbit characterization of Terra MODIS short-wave infrared spectral bands out-of-band responses,” *J. Appl. Remote Sens.*, vol. 14, no. 4, p. 047503, Nov. 2020, doi: 10.1117/1.JRS.14.047503.
[12] Q. Mu *et al.*, “Optimization of a Deep Convective Cloud Technique in Evaluating the Long-Term Radiometric Stability of MODIS Reflective Solar Bands,” *Remote Sens.*, vol. 9, no. 6, p. 535, May 2017, doi: 10.3390/rs9060535.
[13] A. Angal, X. Xiong, Q. Mu, D. R. Doelling, R. Bhatt, and A. Wu, “Results From the Deep Convective Clouds-Based Response Versus Scan-Angle Characterization for the MODIS Reflective Solar Bands,” *IEEE Trans. Geosci. Remote Sens.*, vol. 56, no. 2, pp. 1115–1128, Feb. 2018, doi: 10.1109/TGRS.2017.2759660.
[14] T. M. Wilson, E. Aldoretta, A. Angal, X. Geng, K. Twedt, and X. Xiong, “Analysis of the on-orbit response-versus-scan-angle for the MODIS SWIR bands derived from lunar observations,” in *Proceedings of SPIE*, Sep. 2020, vol. 11530, p. 115301E, doi: 10.1117/12.2572877.
[15] X. Geng, A. Angal, Y. Li, K. A. Twedt, and X. Xiong, “Improvements in the on-orbit response versus scan-angle characterization for the MODIS ocean color bands,” in *Proceedings of SPIE*, Oct. 2019, vol. 11151, p. 1115124, doi: 10.1117/12.2532081.
[16] Z. Wang and X. Xiong, “Band-to-Band Misregistration of the Images of MODIS Onboard Calibrators and Its Impact on Calibration,” *IEEE Trans. Geosci. Remote Sens.*, vol. 55, no. 4, pp. 2136–2143, Apr. 2017, doi: 10.1109/TGRS.2016.2637167.
[17] Z. Wang, X. Xiong, and W. L. Barnes, “Further investigation on MODIS solar diffuser screen vignetting function and its implementation in RSB calibration,” in *Proceedings of SPIE*, Sep. 2011, vol. 8153, p. 815307, doi: 10.1117/12.892482.
[18] Q. Mu, A. Angal, K. Twedt, A. Wu, and X. Xiong, “MODIS detector differences using deep convective clouds and desert targets,” in *Proceedings of SPIE*, Sep. 2020, vol. 11530, p. 115301A, doi: 10.1117/12.2571977.
[19] J.-Q. Sun, X. Xiong, W. L. Barnes, and B. Guenther, “MODIS Reflective Solar Bands On-Orbit Lunar Calibration,” *IEEE Trans. Geosci. Remote Sens.*, vol. 45, no. 7, pp. 2383–2393, Jul. 2007, doi: 10.1109/TGRS.2007.896541.

APPENDIX A. C6.1 vs. C7 m_1/RVS comparison plots

The following plots show the ratio of the calibrated m_1/RVS (inverse gain) between C6.1 and C7. The plots show difference trends for each band over the entire Terra and Aqua missions for each band (averaged over all detectors and subframes within a band; noisy and dead detectors are excluded from the average). Trends are shown at multiple EV frames to demonstrate the combined changes to both m_1 and RVS.

As stated in Section 3, the Terra short wavelength bands (3,8-12) and SWIR bands (5-7, 26) have the most significant differences between C6.1 and C7. For all other Terra bands and all Aqua bands, the C7-C6.1 differences are generally within 1% on average. In many cases, there are short time periods after the start of C6 (2012) where the C7-C6.1 differences are up to 2% or so even for bands with no major algorithm changes. This is due to short-term errors in the forward predicted LUTs used in C6. The C7 LUTs are reprocessed over the entire mission with consistent algorithms, which will correct these slight deviations.

A.1 Terra MODIS

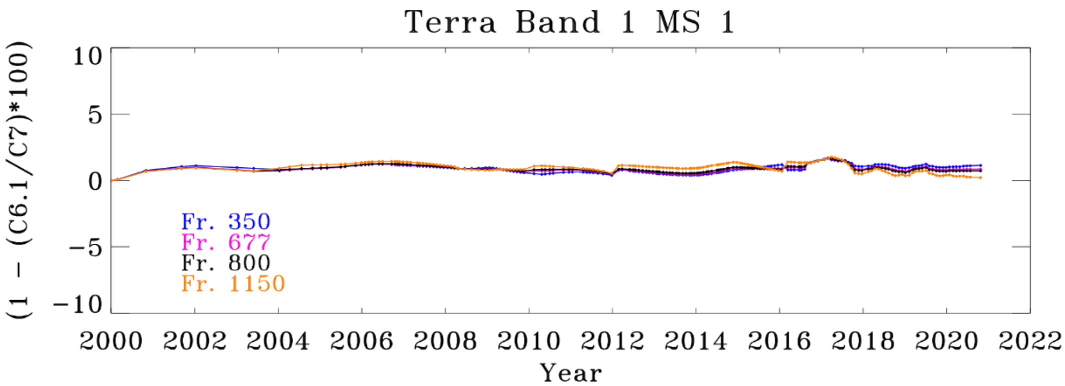

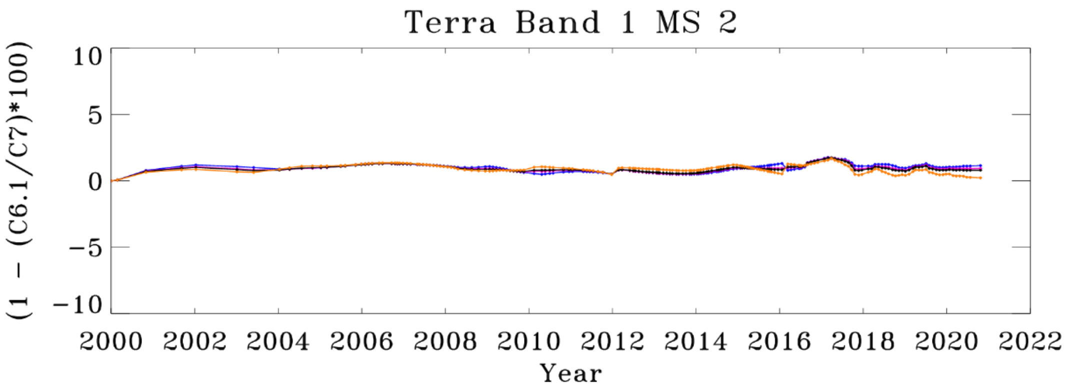

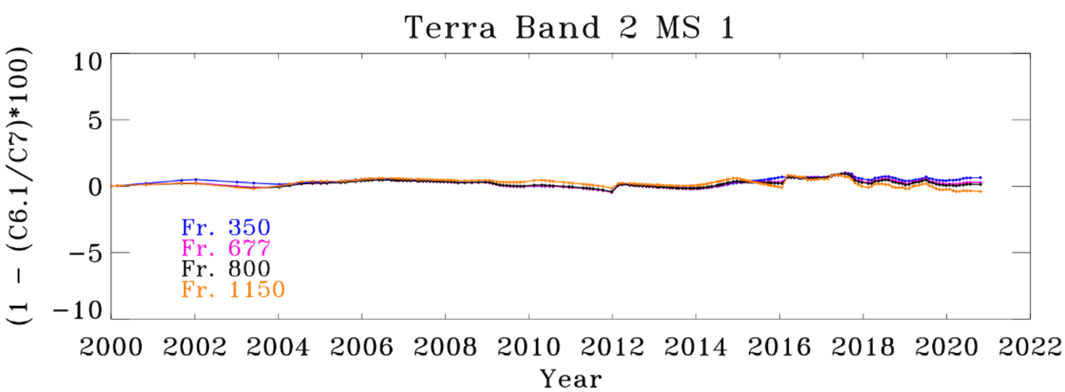

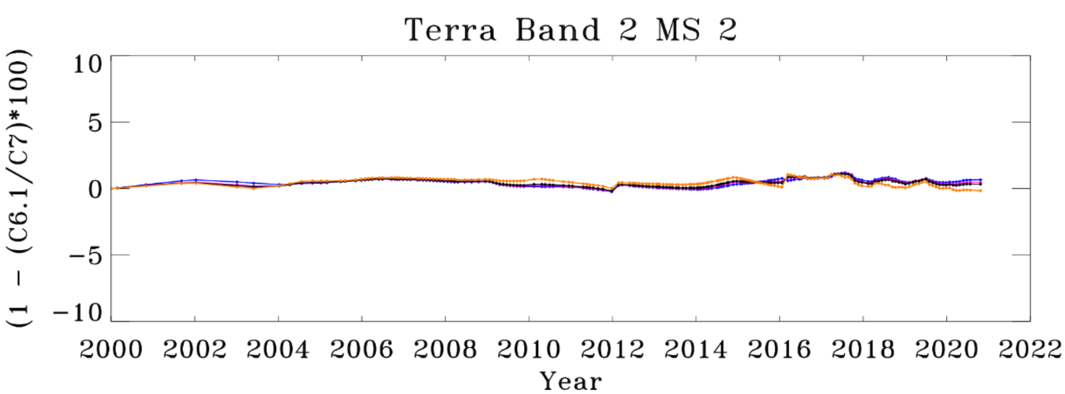

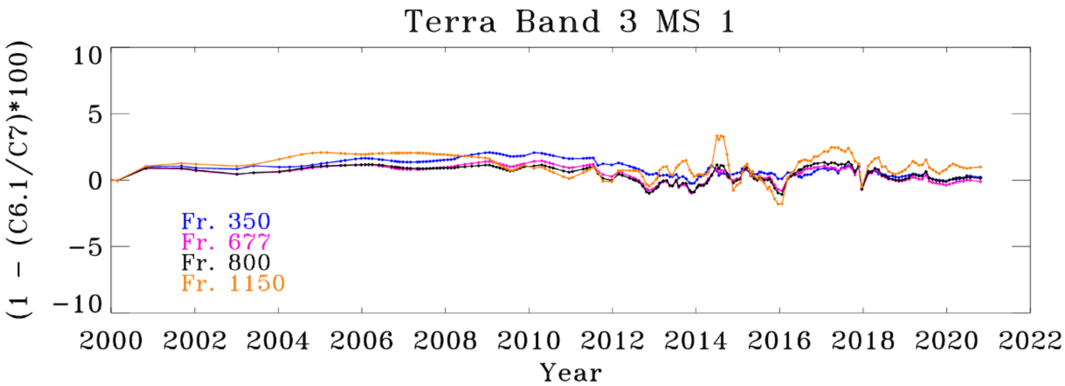
Terra Band 3 MS 1
(1 − (C6.1/C7)*100)
Fr. 350
Fr. 677
Fr. 800
Fr. 1150
Year

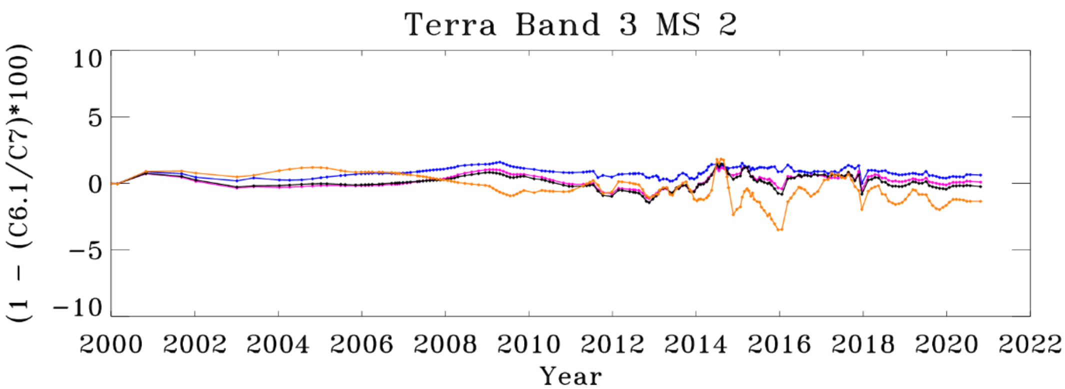
Terra Band 3 MS 2
(1 − (C6.1/C7)*100)
Year

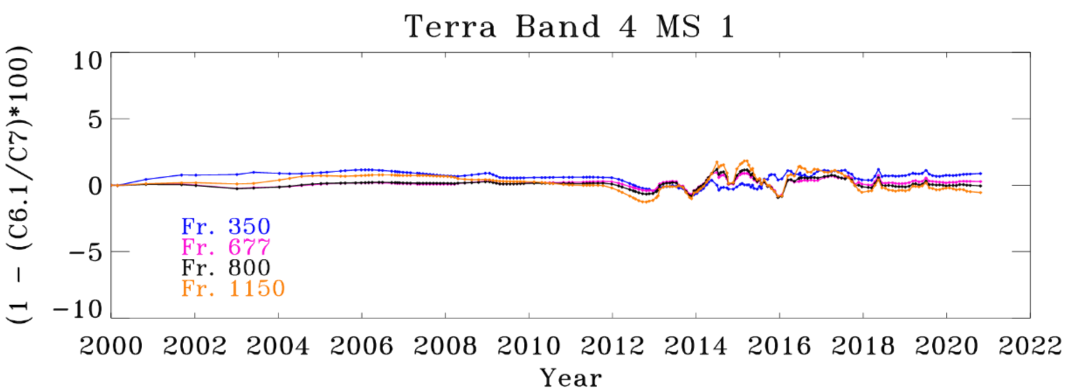
Terra Band 4 MS 1
(1 − (C6.1/C7)*100)
Fr. 350
Fr. 677
Fr. 800
Fr. 1150
Year

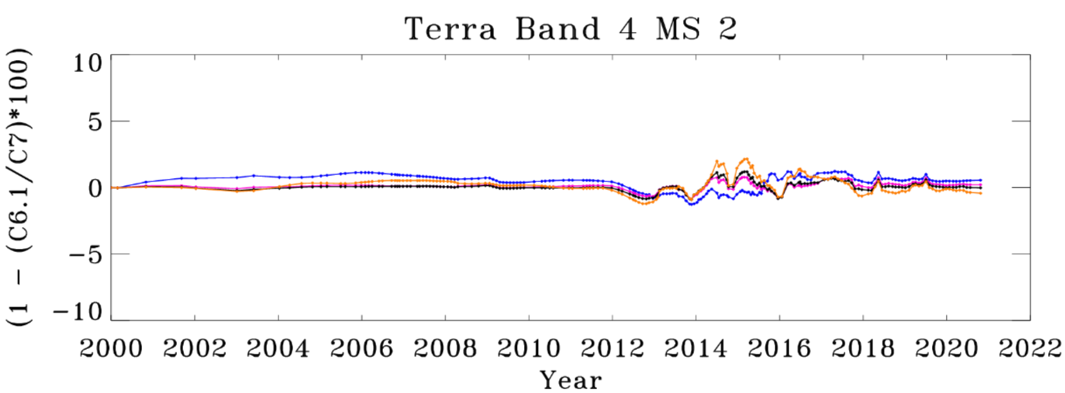
Terra Band 4 MS 2
(1 − (C6.1/C7)*100)
Year

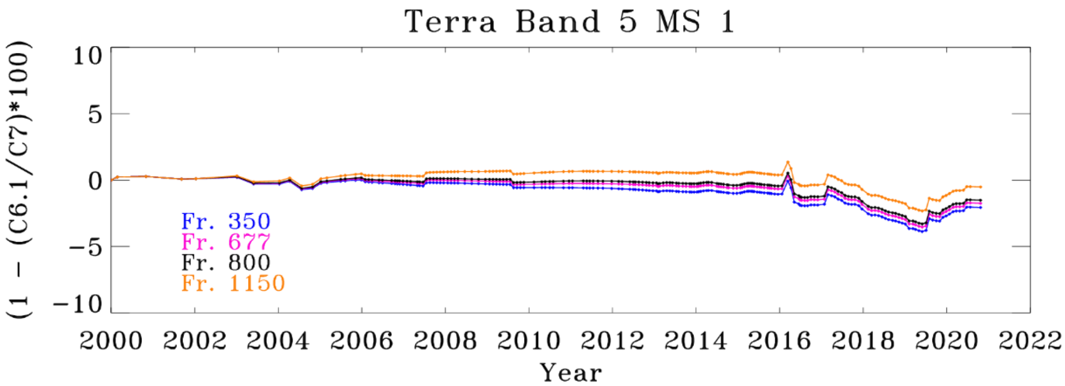
Terra Band 5 MS 1
(1 − (C6.1/C7)*100)
10
5
0
−5
−10
Fr. 350
Fr. 677
Fr. 800
Fr. 1150
2000 2002 2004 2006 2008 2010 2012 2014 2016 2018 2020 2022
Year

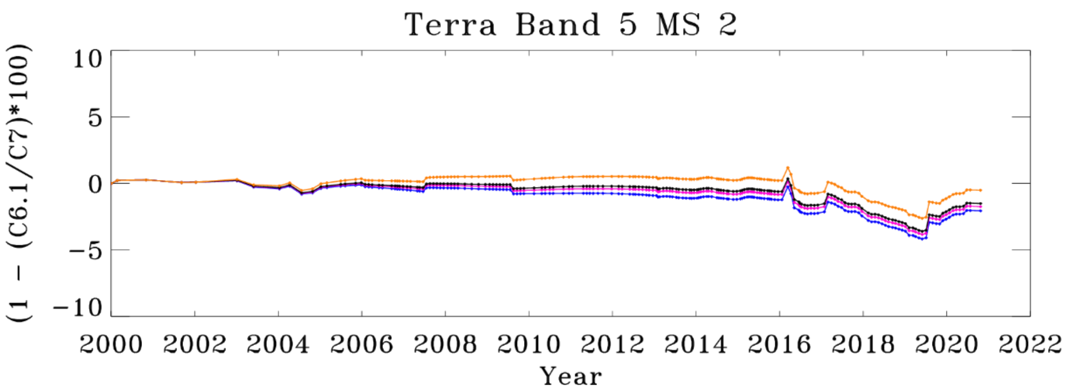
Terra Band 5 MS 2
(1 − (C6.1/C7)*100)
10
5
0
−5
−10
2000 2002 2004 2006 2008 2010 2012 2014 2016 2018 2020 2022
Year

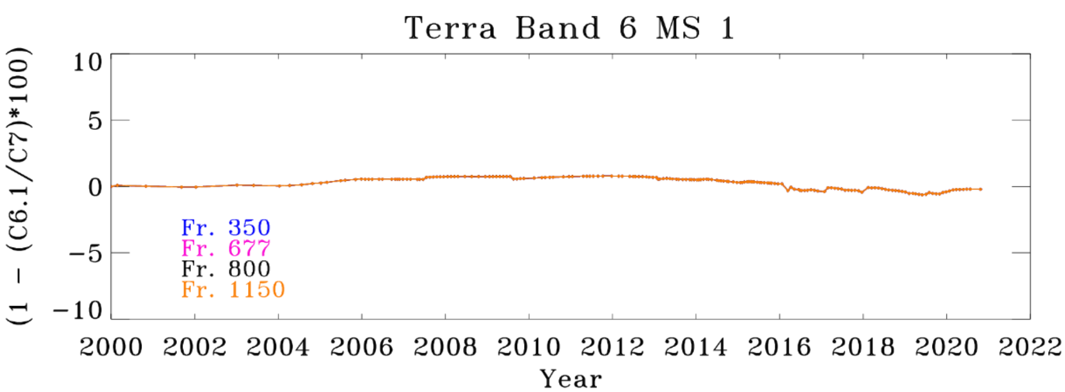
Terra Band 6 MS 1
(1 − (C6.1/C7)*100)
10
5
0
−5
−10
Fr. 350
Fr. 677
Fr. 800
Fr. 1150
2000 2002 2004 2006 2008 2010 2012 2014 2016 2018 2020 2022
Year

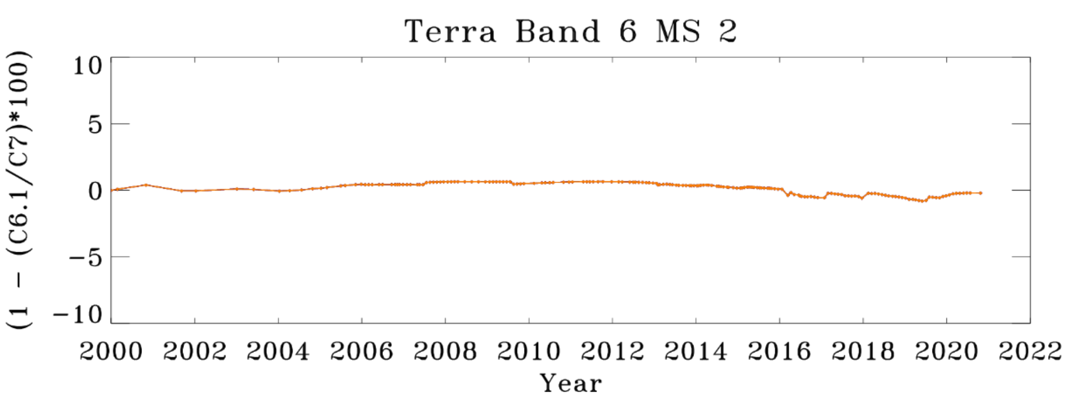
Terra Band 6 MS 2
(1 − (C6.1/C7)*100)
10
5
0
−5
−10
2000 2002 2004 2006 2008 2010 2012 2014 2016 2018 2020 2022
Year

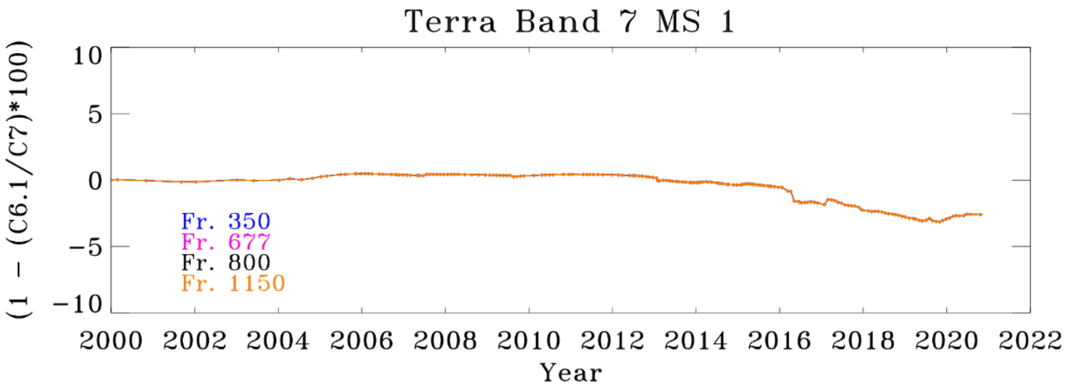

Terra Band 7 MS 1
(1 − (C6.1/C7)*100)
10
5
0
−5
−10
Fr. 350
Fr. 677
Fr. 800
Fr. 1150
2000 2002 2004 2006 2008 2010 2012 2014 2016 2018 2020 2022
Year

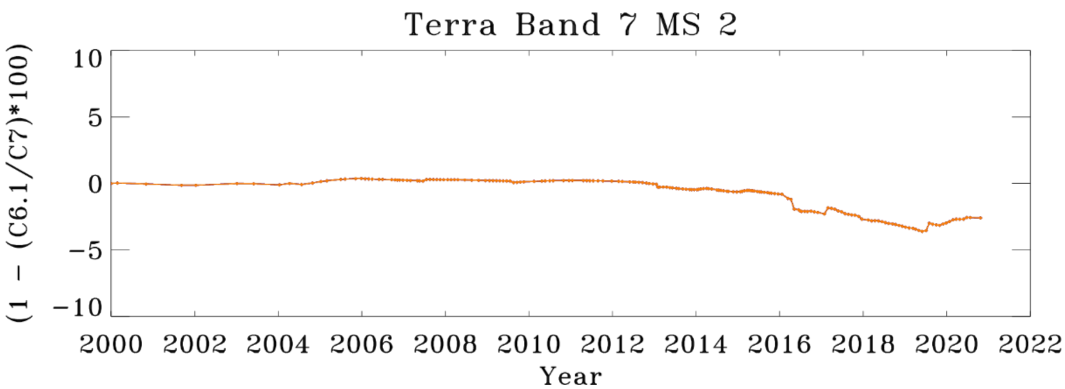

Terra Band 7 MS 2
(1 − (C6.1/C7)*100)
10
5
0
−5
−10
2000 2002 2004 2006 2008 2010 2012 2014 2016 2018 2020 2022
Year

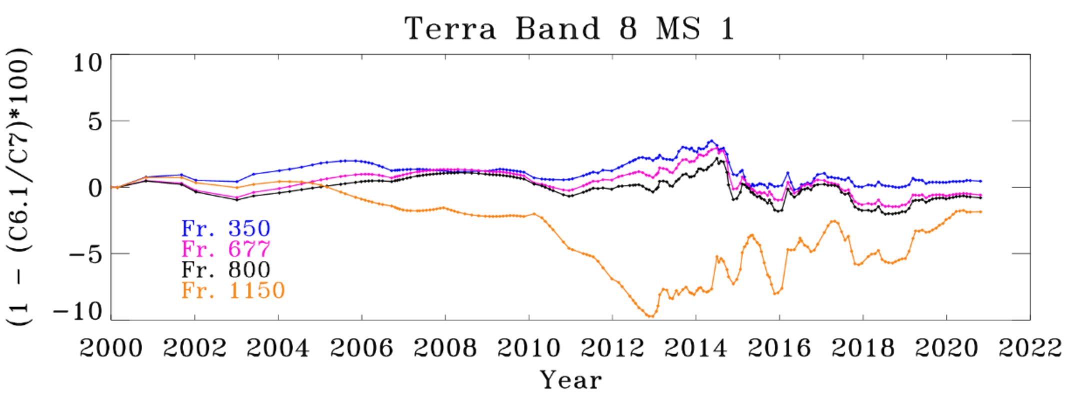

Terra Band 8 MS 1
(1 − (C6.1/C7)*100)
10
5
0
−5
−10
Fr. 350
Fr. 677
Fr. 800
Fr. 1150
2000 2002 2004 2006 2008 2010 2012 2014 2016 2018 2020 2022
Year

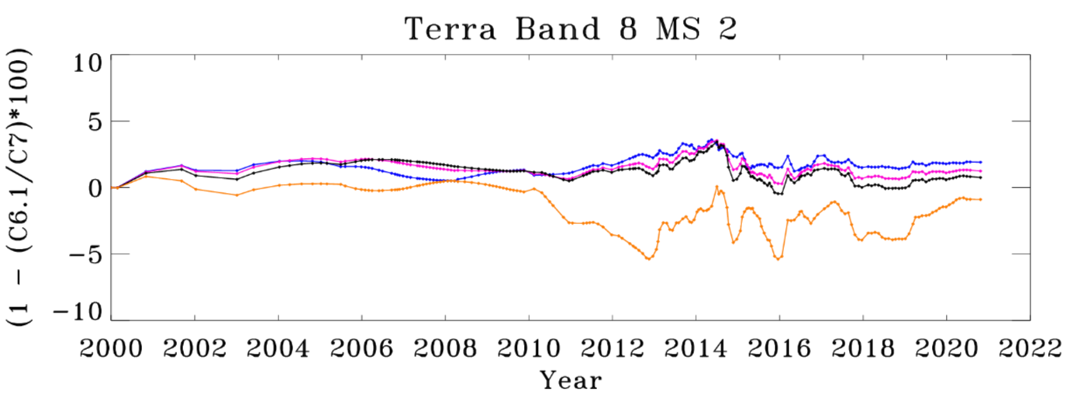

Terra Band 8 MS 2
(1 − (C6.1/C7)*100)
10
5
0
−5
−10
2000 2002 2004 2006 2008 2010 2012 2014 2016 2018 2020 2022
Year

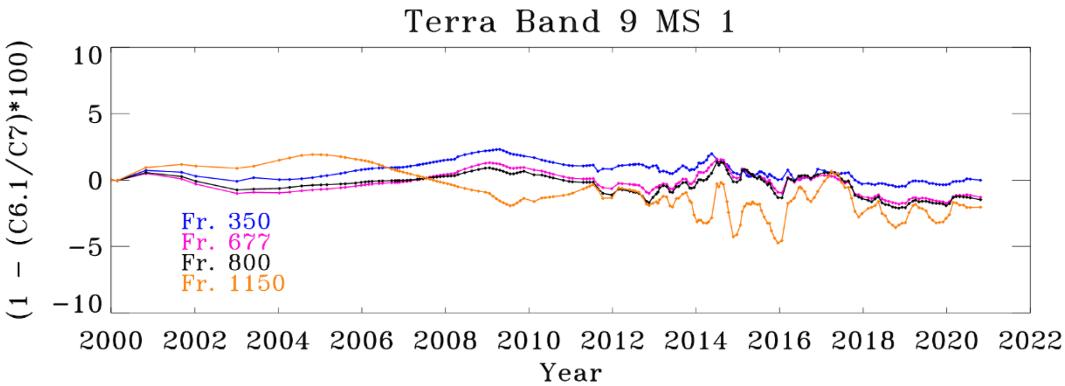
Terra Band 9 MS 1
(1 − (C6.1/C7)*100)
10
5
0
−5
−10
2000 2002 2004 2006 2008 2010 2012 2014 2016 2018 2020 2022
Year
Fr. 350
Fr. 677
Fr. 800
Fr. 1150

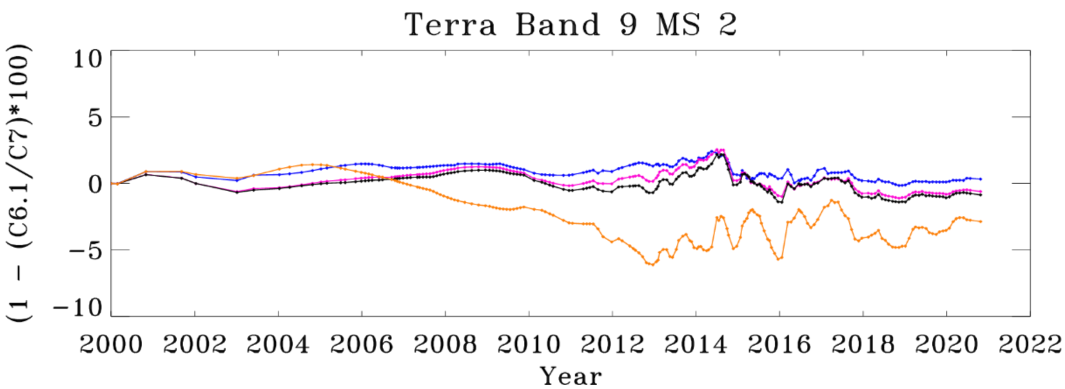
Terra Band 9 MS 2
(1 − (C6.1/C7)*100)
10
5
0
−5
−10
2000 2002 2004 2006 2008 2010 2012 2014 2016 2018 2020 2022
Year

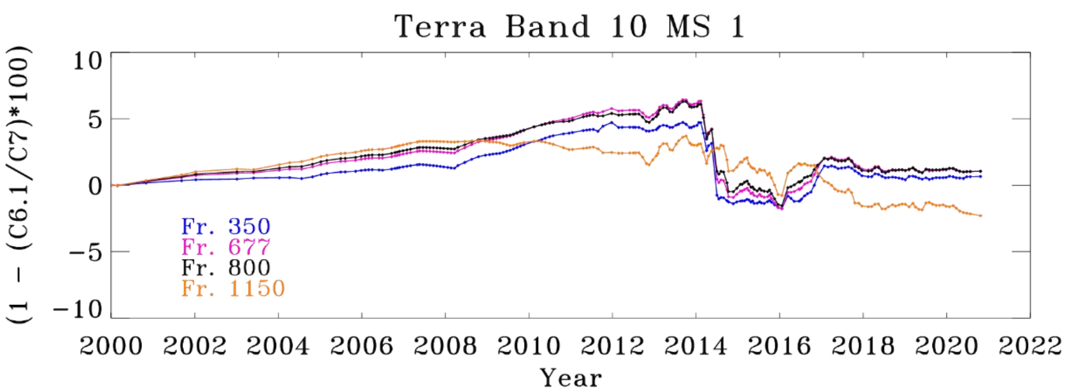
Terra Band 10 MS 1
(1 − (C6.1/C7)*100)
10
5
0
−5
−10
2000 2002 2004 2006 2008 2010 2012 2014 2016 2018 2020 2022
Year
Fr. 350
Fr. 677
Fr. 800
Fr. 1150

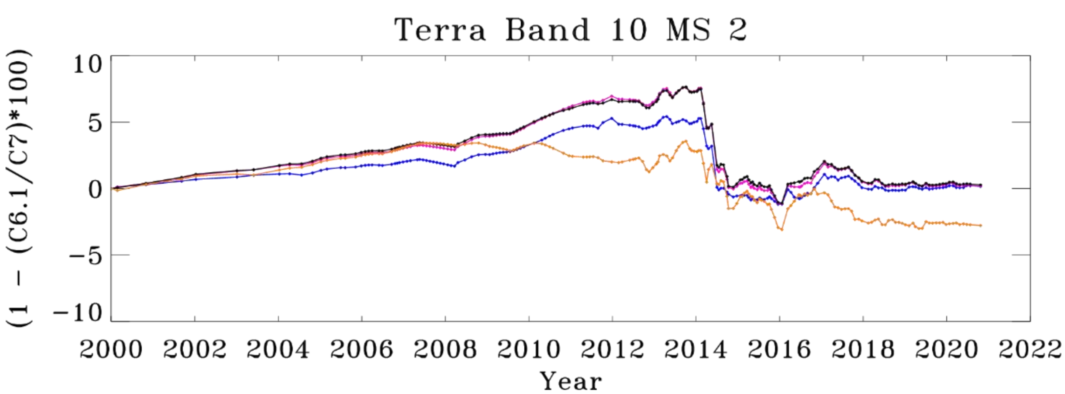
Terra Band 10 MS 2
(1 − (C6.1/C7)*100)
10
5
0
−5
−10
2000 2002 2004 2006 2008 2010 2012 2014 2016 2018 2020 2022
Year

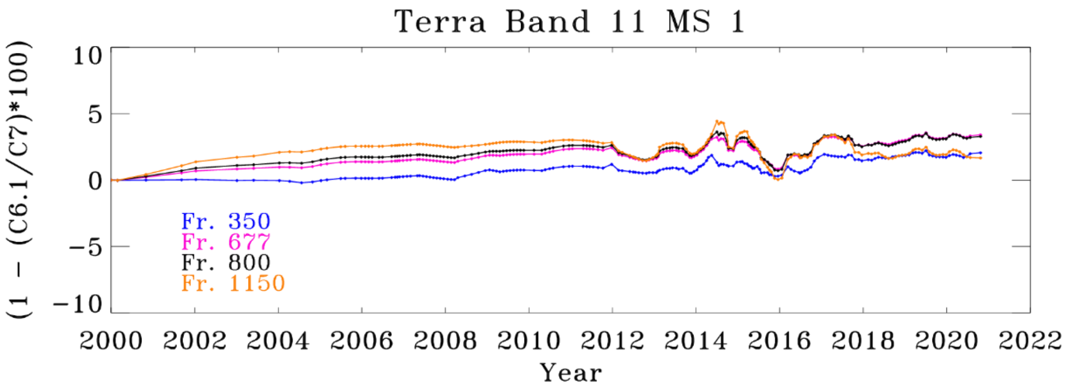
Terra Band 11 MS 1
(1 − (C6.1/C7)*100)
Year
Fr. 350
Fr. 677
Fr. 800
Fr. 1150

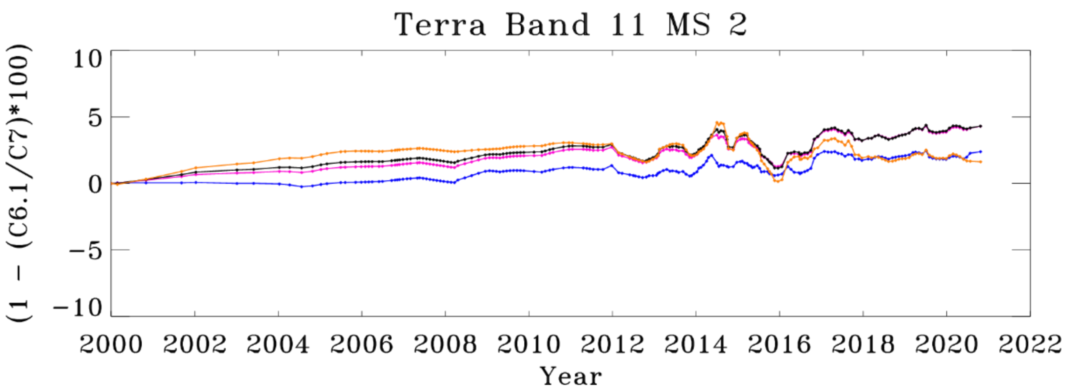
Terra Band 11 MS 2
(1 − (C6.1/C7)*100)
Year

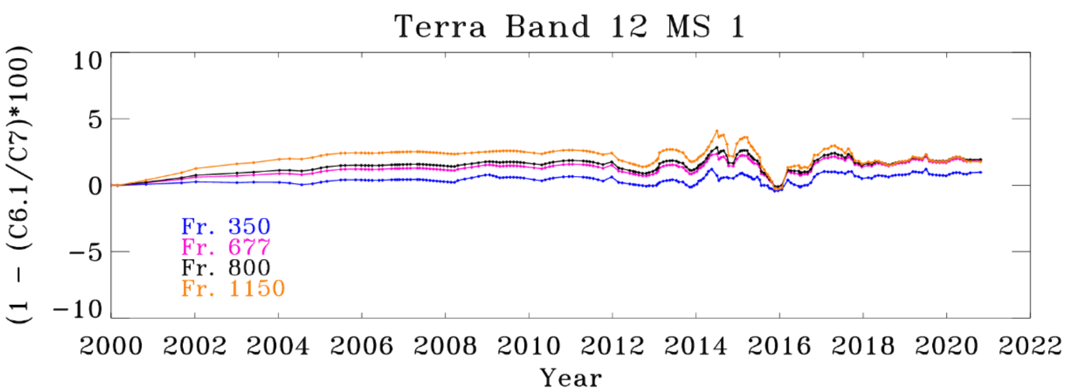
Terra Band 12 MS 1
(1 − (C6.1/C7)*100)
Year
Fr. 350
Fr. 677
Fr. 800
Fr. 1150

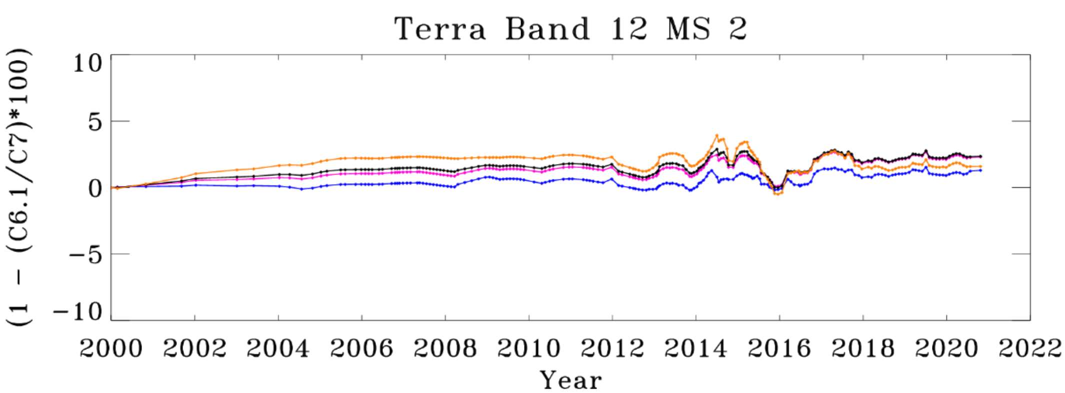
Terra Band 12 MS 2
(1 − (C6.1/C7)*100)
Year

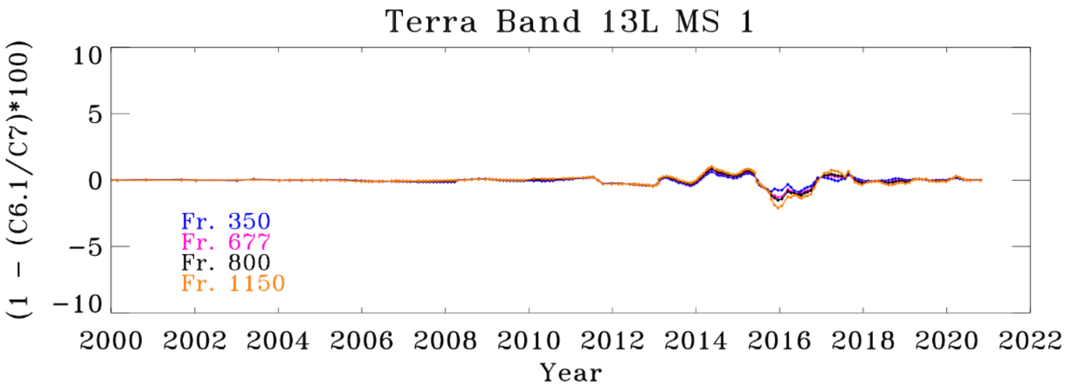
Terra Band 13L MS 1
(1 − (C6.1/C7)*100)
10
5
0
−5
−10
2000 2002 2004 2006 2008 2010 2012 2014 2016 2018 2020 2022
Year
Fr. 350
Fr. 677
Fr. 800
Fr. 1150

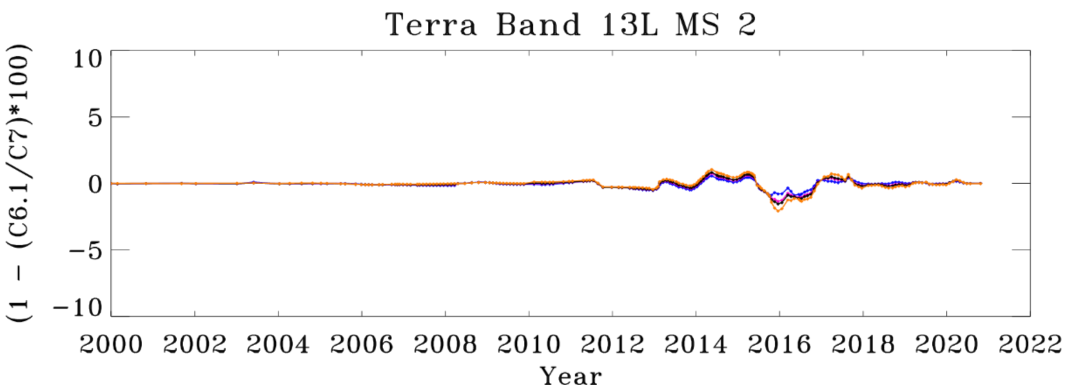
Terra Band 13L MS 2
(1 − (C6.1/C7)*100)
10
5
0
−5
−10
2000 2002 2004 2006 2008 2010 2012 2014 2016 2018 2020 2022
Year

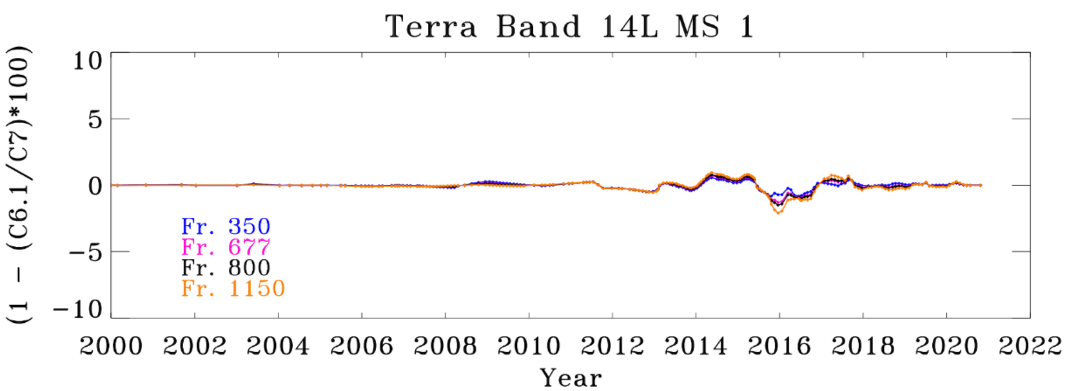
Terra Band 14L MS 1
(1 − (C6.1/C7)*100)
10
5
0
−5
−10
2000 2002 2004 2006 2008 2010 2012 2014 2016 2018 2020 2022
Year
Fr. 350
Fr. 677
Fr. 800
Fr. 1150

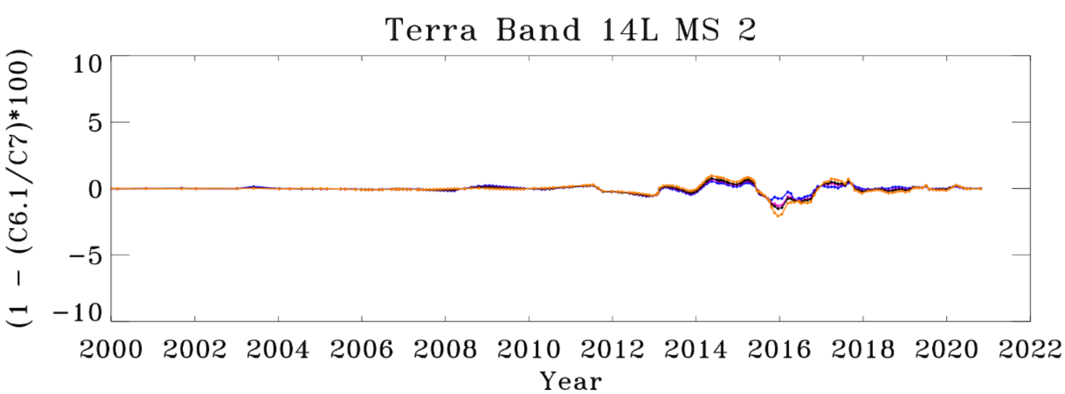
Terra Band 14L MS 2
(1 − (C6.1/C7)*100)
10
5
0
−5
−10
2000 2002 2004 2006 2008 2010 2012 2014 2016 2018 2020 2022
Year

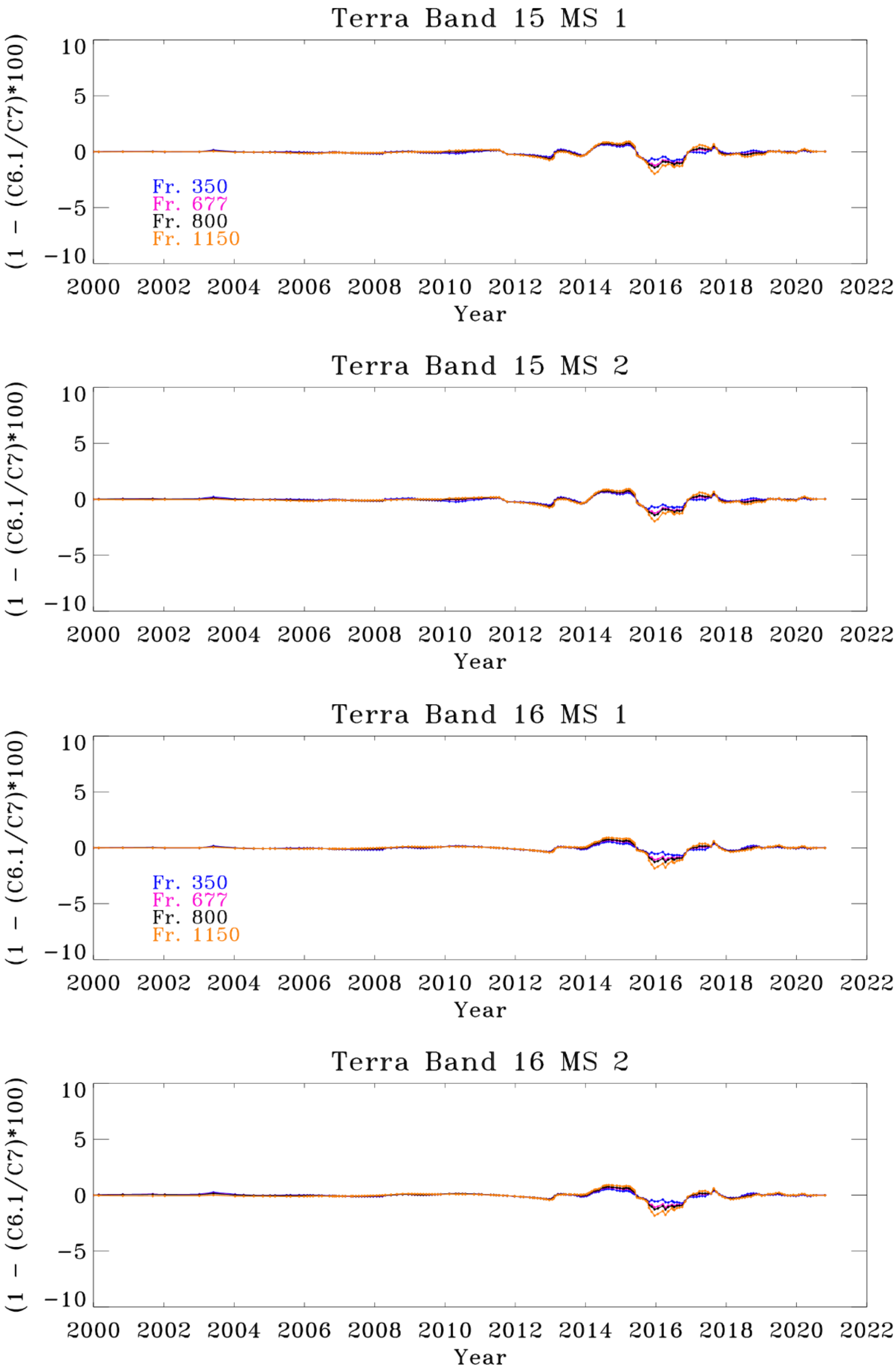

Terra Band 15 MS 1
(1 − (C6.1/C7)*100)
10
5
0
−5
−10
Fr. 350
Fr. 677
Fr. 800
Fr. 1150
2000 2002 2004 2006 2008 2010 2012 2014 2016 2018 2020 2022
Year
Terra Band 15 MS 2
(1 − (C6.1/C7)*100)
10
5
0
−5
−10
2000 2002 2004 2006 2008 2010 2012 2014 2016 2018 2020 2022
Year
Terra Band 16 MS 1
(1 − (C6.1/C7)*100)
10
5
0
−5
−10
Fr. 350
Fr. 677
Fr. 800
Fr. 1150
2000 2002 2004 2006 2008 2010 2012 2014 2016 2018 2020 2022
Year
Terra Band 16 MS 2
(1 − (C6.1/C7)*100)
10
5
0
−5
−10
2000 2002 2004 2006 2008 2010 2012 2014 2016 2018 2020 2022
Year

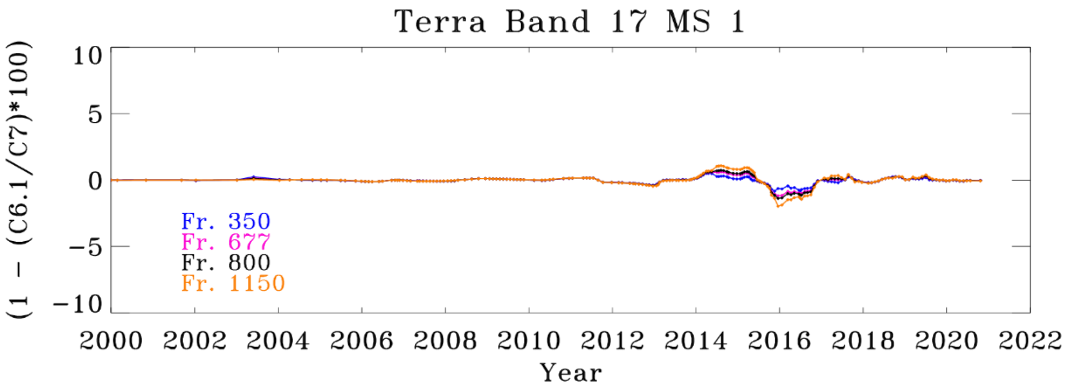
Terra Band 17 MS 1
(1 − (C6.1/C7)*100)
Year
Fr. 350
Fr. 677
Fr. 800
Fr. 1150

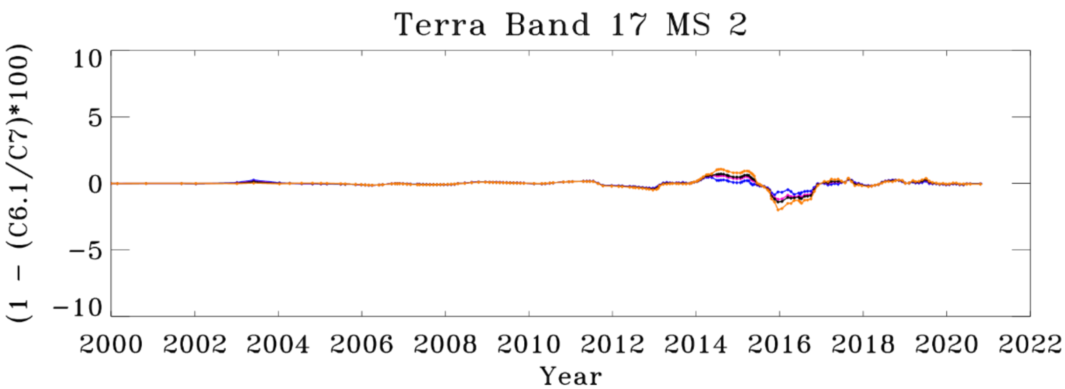
Terra Band 17 MS 2
(1 − (C6.1/C7)*100)
Year

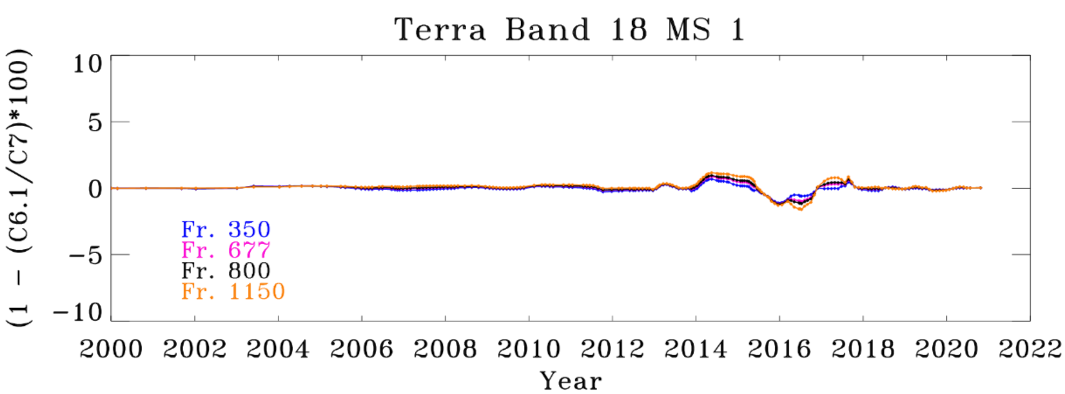
Terra Band 18 MS 1
(1 − (C6.1/C7)*100)
Year
Fr. 350
Fr. 677
Fr. 800
Fr. 1150

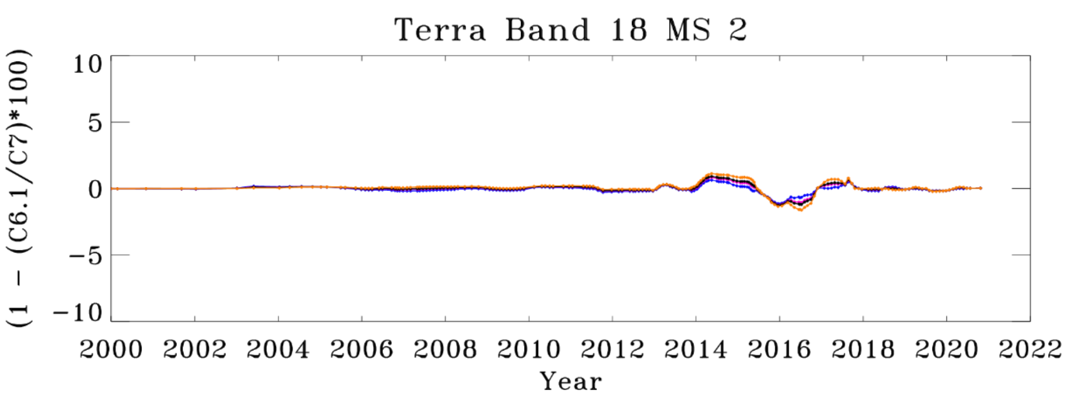
Terra Band 18 MS 2
(1 − (C6.1/C7)*100)
Year

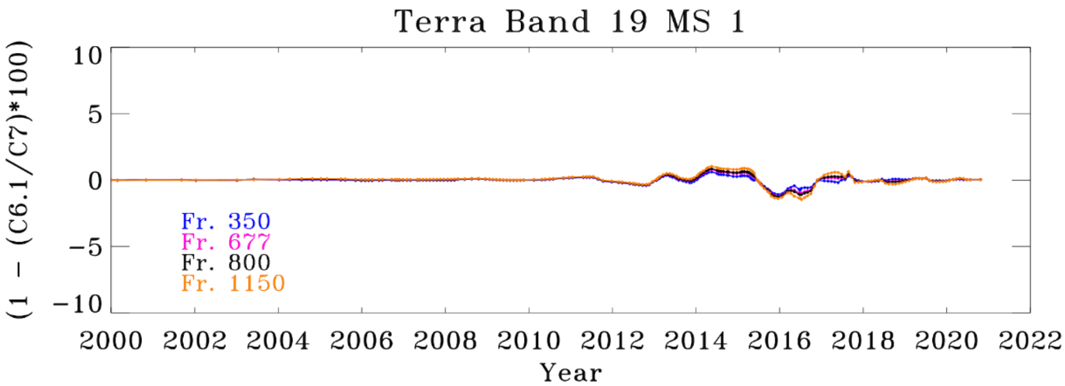
Terra Band 19 MS 1
(1 − (C6.1/C7)*100)
Year
Fr. 350
Fr. 677
Fr. 800
Fr. 1150

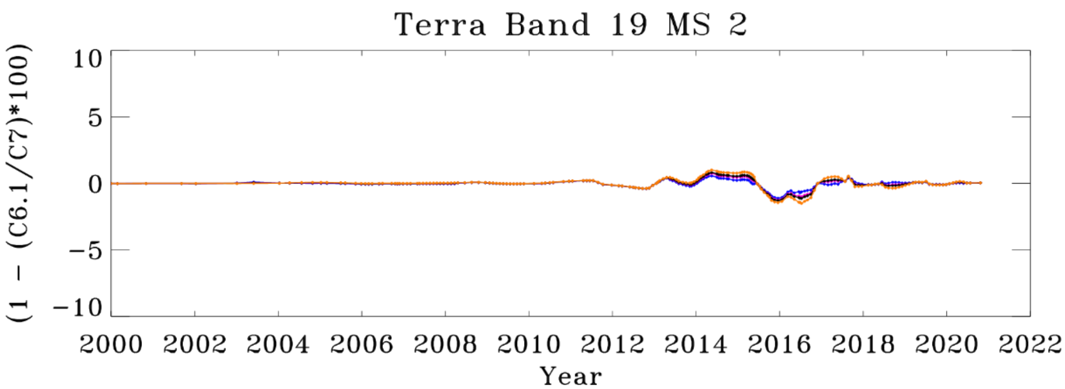
Terra Band 19 MS 2
(1 − (C6.1/C7)*100)
Year

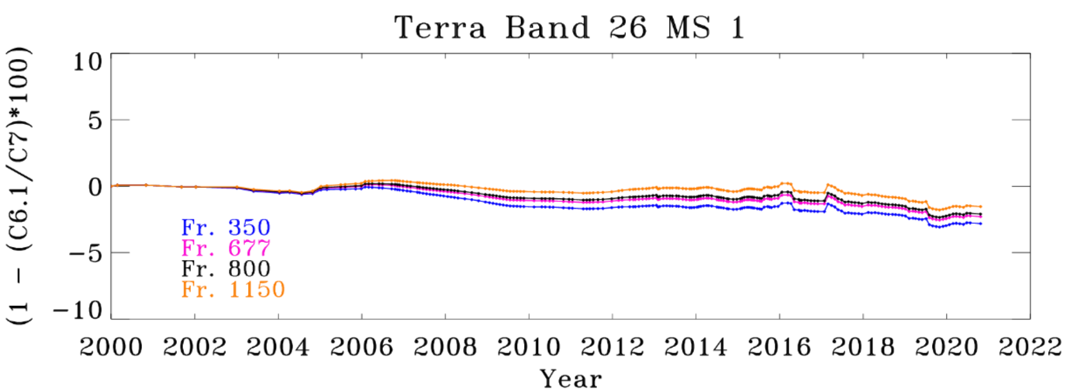
Terra Band 26 MS 1
(1 − (C6.1/C7)*100)
Year
Fr. 350
Fr. 677
Fr. 800
Fr. 1150

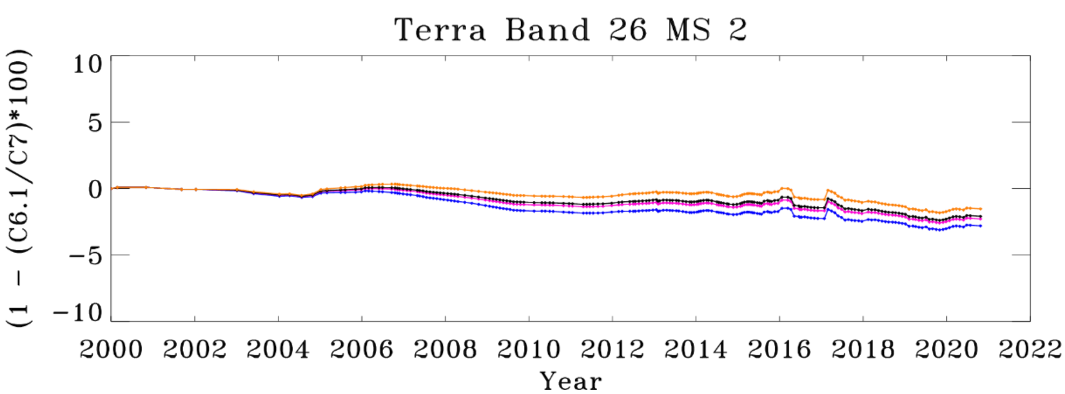
Terra Band 26 MS 2
(1 − (C6.1/C7)*100)
Year

A.2 Aqua MODIS

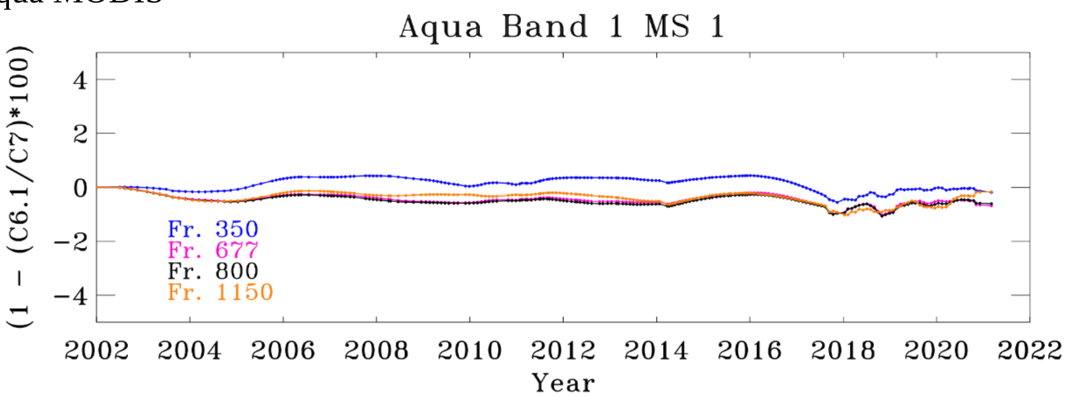

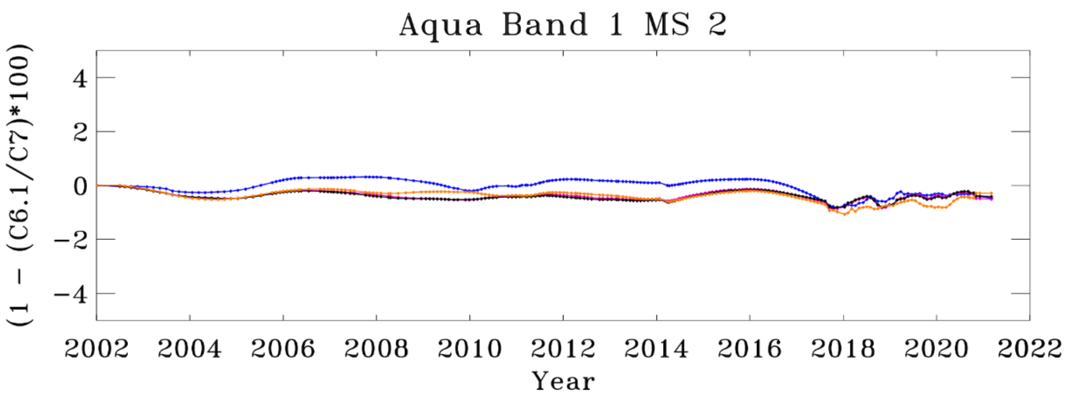

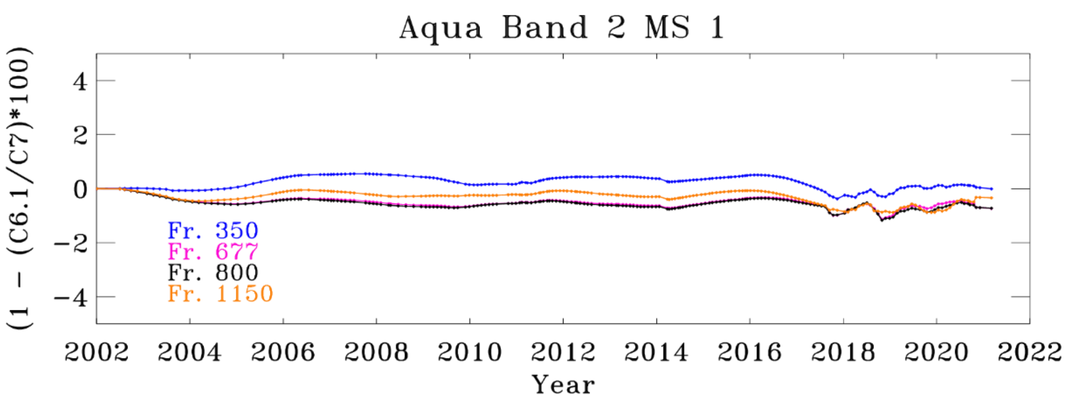

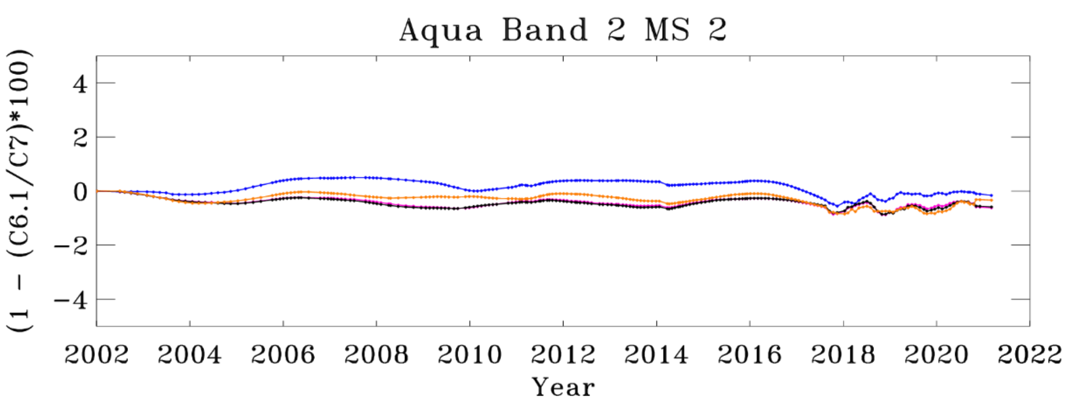

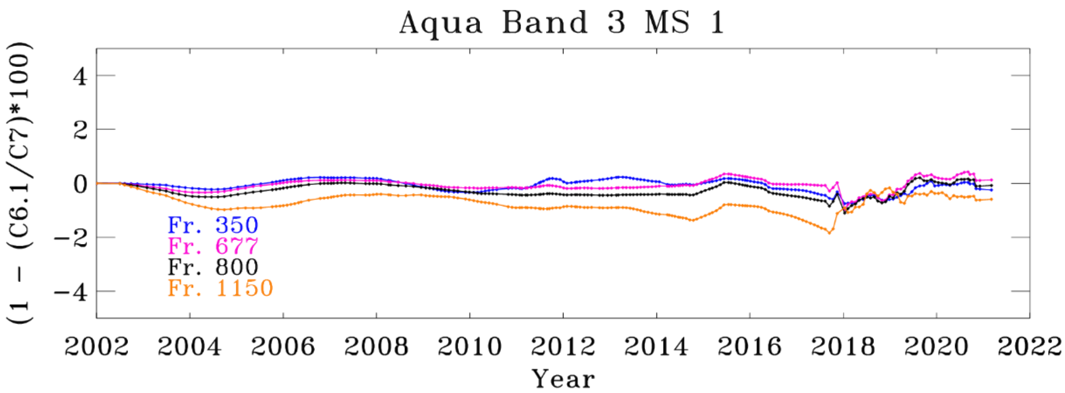
Aqua Band 3 MS 1
(1 − (C6.1/C7)*100)
4
2
0
−2
−4
Fr. 350
Fr. 677
Fr. 800
Fr. 1150
2002
2004
2006
2008
2010
2012
2014
2016
2018
2020
2022
Year

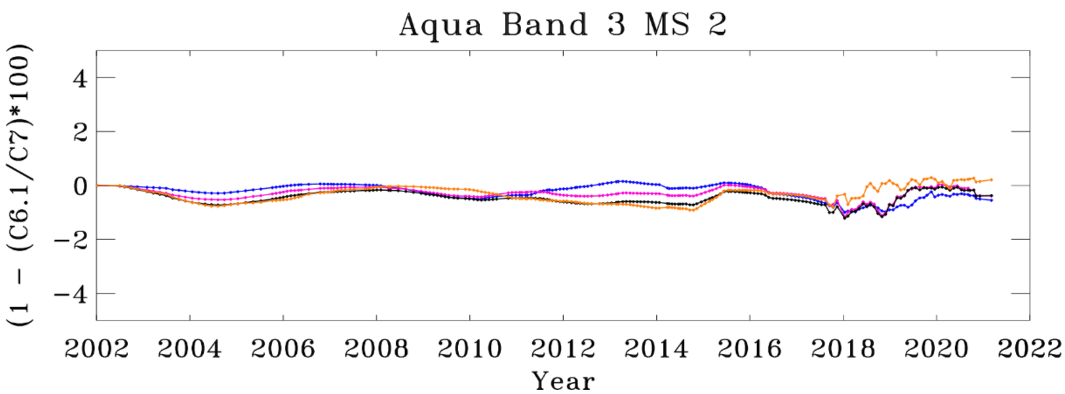
Aqua Band 3 MS 2
(1 − (C6.1/C7)*100)
4
2
0
−2
−4
2002
2004
2006
2008
2010
2012
2014
2016
2018
2020
2022
Year

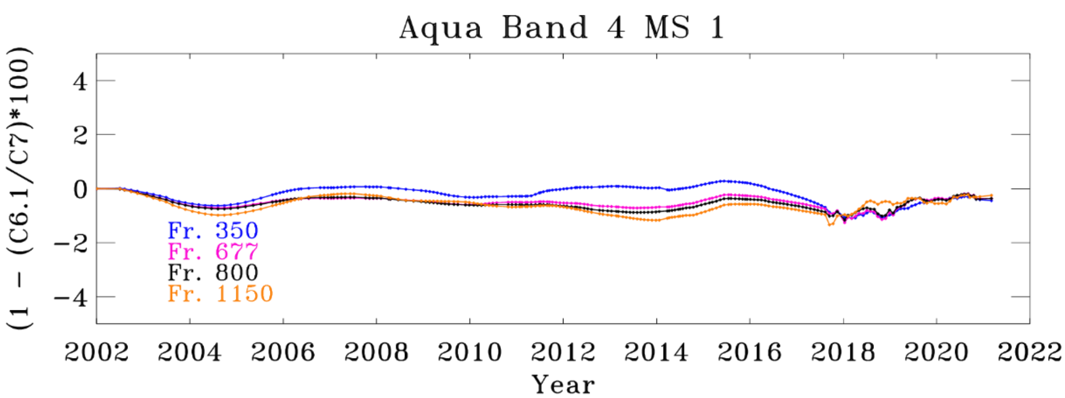
Aqua Band 4 MS 1
(1 − (C6.1/C7)*100)
4
2
0
−2
−4
Fr. 350
Fr. 677
Fr. 800
Fr. 1150
2002
2004
2006
2008
2010
2012
2014
2016
2018
2020
2022
Year

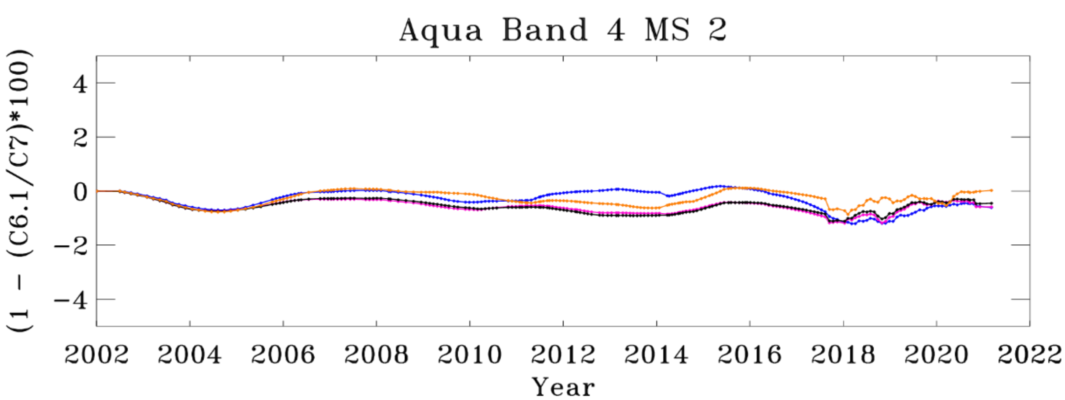
Aqua Band 4 MS 2
(1 − (C6.1/C7)*100)
4
2
0
−2
−4
2002
2004
2006
2008
2010
2012
2014
2016
2018
2020
2022
Year

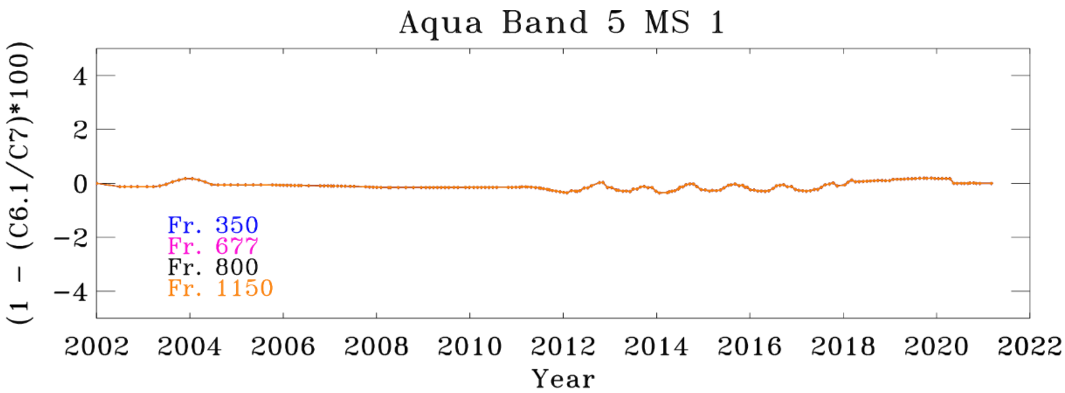
Aqua Band 5 MS 1
(1 − (C6.1/C7)*100)
Year
Fr. 350
Fr. 677
Fr. 800
Fr. 1150

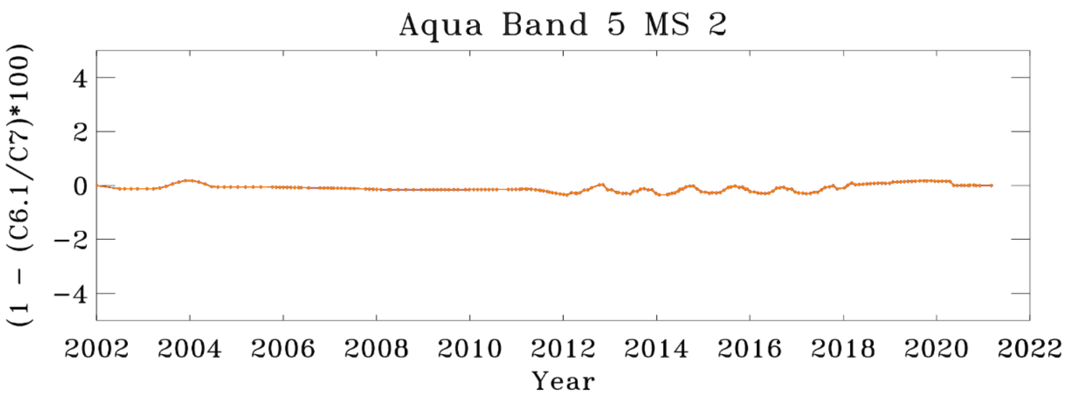
Aqua Band 5 MS 2
(1 − (C6.1/C7)*100)
Year

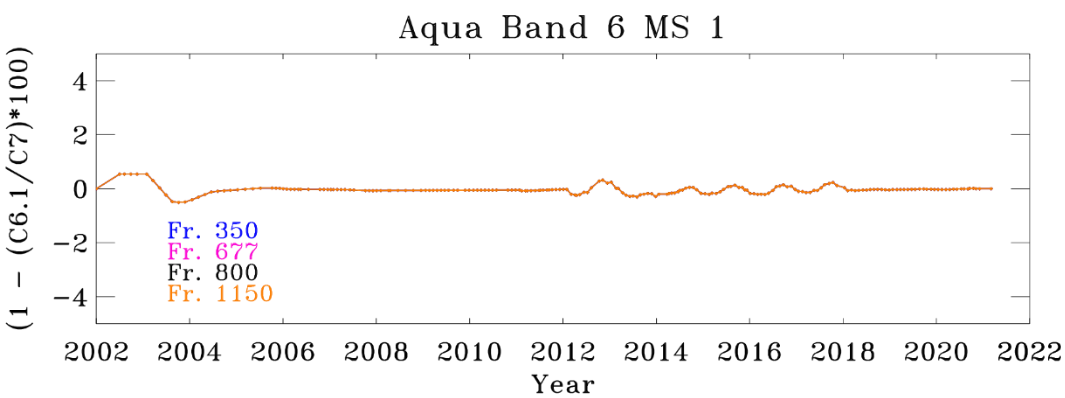
Aqua Band 6 MS 1
(1 − (C6.1/C7)*100)
Year
Fr. 350
Fr. 677
Fr. 800
Fr. 1150

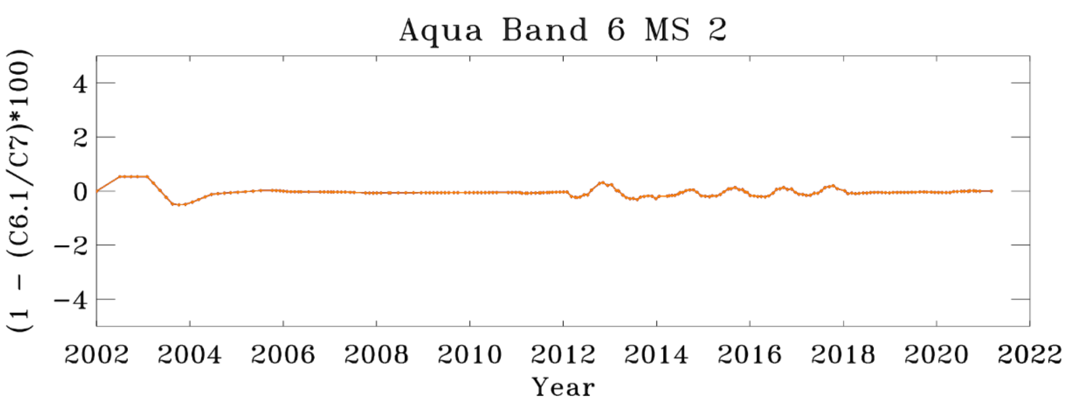
Aqua Band 6 MS 2
(1 − (C6.1/C7)*100)
Year

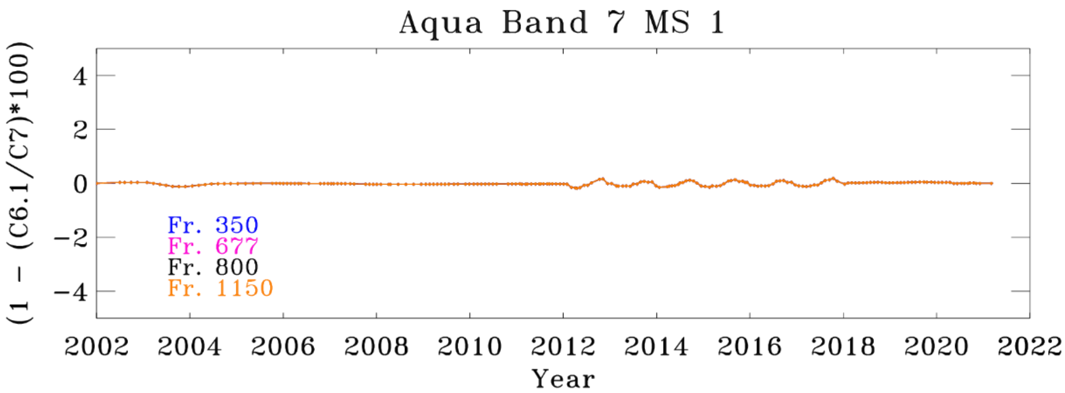
Aqua Band 7 MS 1
(1 − (C6.1/C7)*100)
Year
Fr. 350
Fr. 677
Fr. 800
Fr. 1150

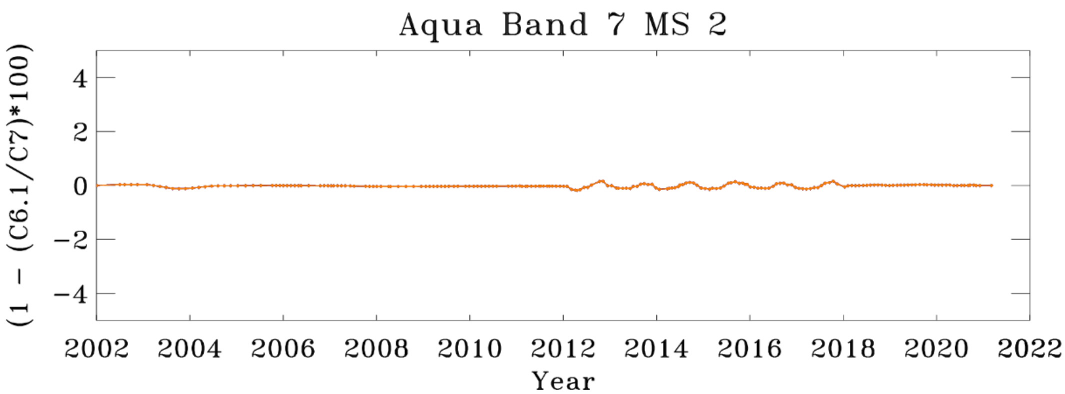
Aqua Band 7 MS 2
(1 − (C6.1/C7)*100)
Year

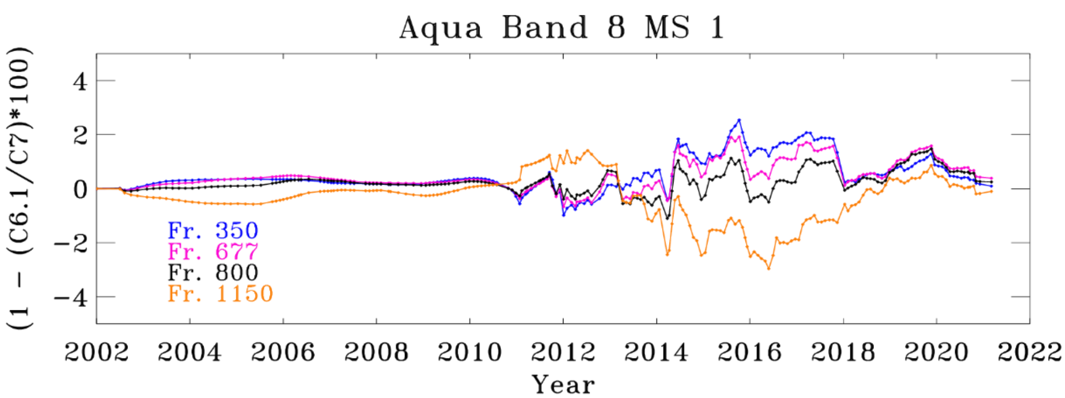
Aqua Band 8 MS 1
(1 − (C6.1/C7)*100)
Year
Fr. 350
Fr. 677
Fr. 800
Fr. 1150

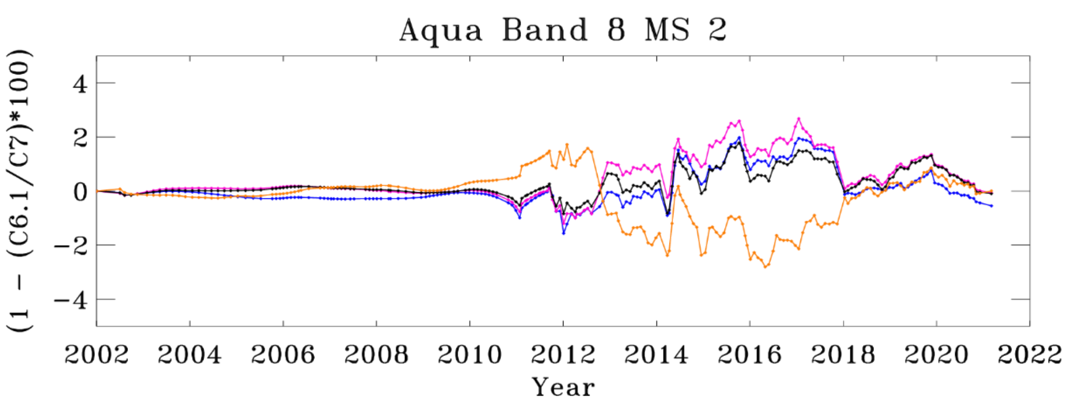
Aqua Band 8 MS 2
(1 − (C6.1/C7)*100)
Year

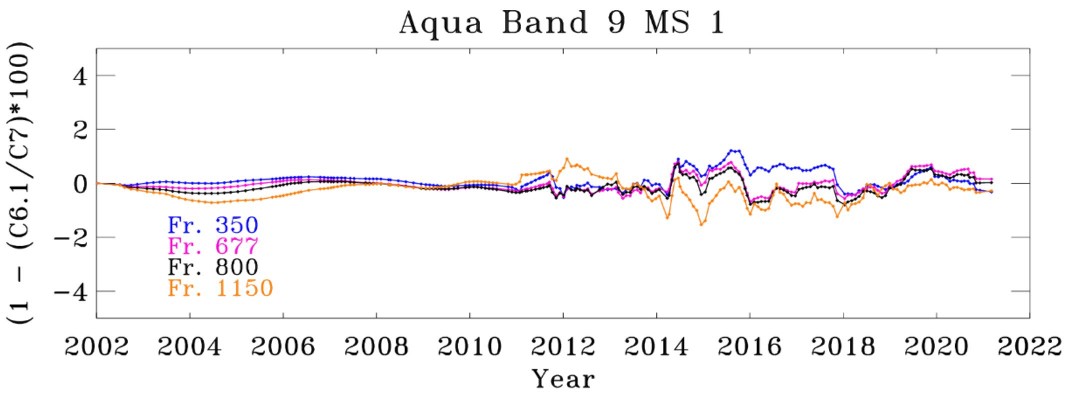
Aqua Band 9 MS 1
(1 − (C6.1/C7)*100)
4
2
0
−2
−4
Fr. 350
Fr. 677
Fr. 800
Fr. 1150
2002
2004
2006
2008
2010
2012
2014
2016
2018
2020
2022
Year

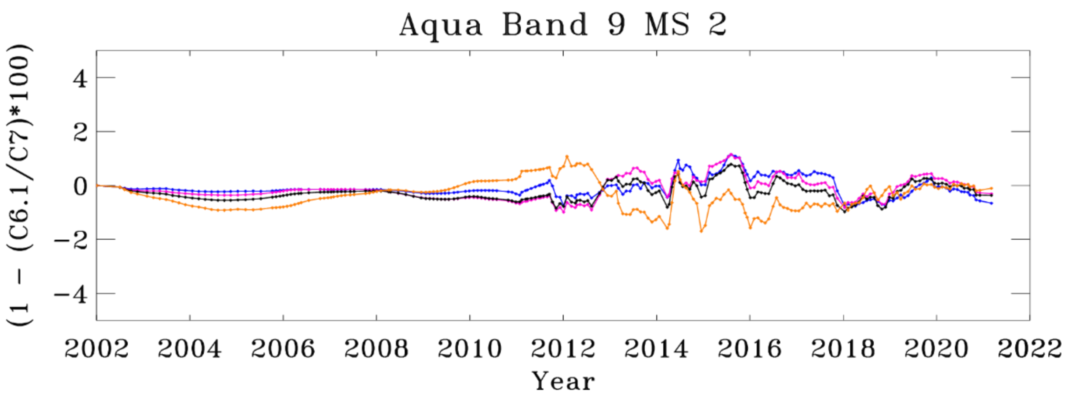
Aqua Band 9 MS 2
(1 − (C6.1/C7)*100)
4
2
0
−2
−4
2002
2004
2006
2008
2010
2012
2014
2016
2018
2020
2022
Year

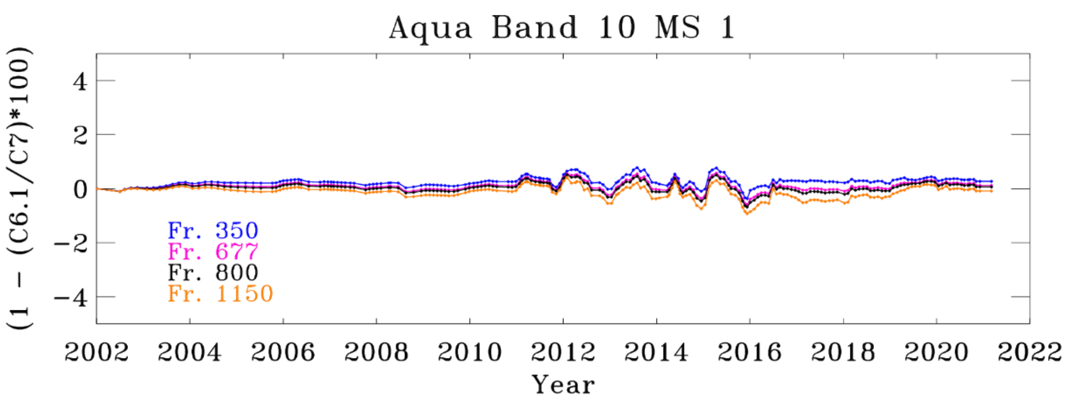
Aqua Band 10 MS 1
(1 − (C6.1/C7)*100)
4
2
0
−2
−4
Fr. 350
Fr. 677
Fr. 800
Fr. 1150
2002
2004
2006
2008
2010
2012
2014
2016
2018
2020
2022
Year

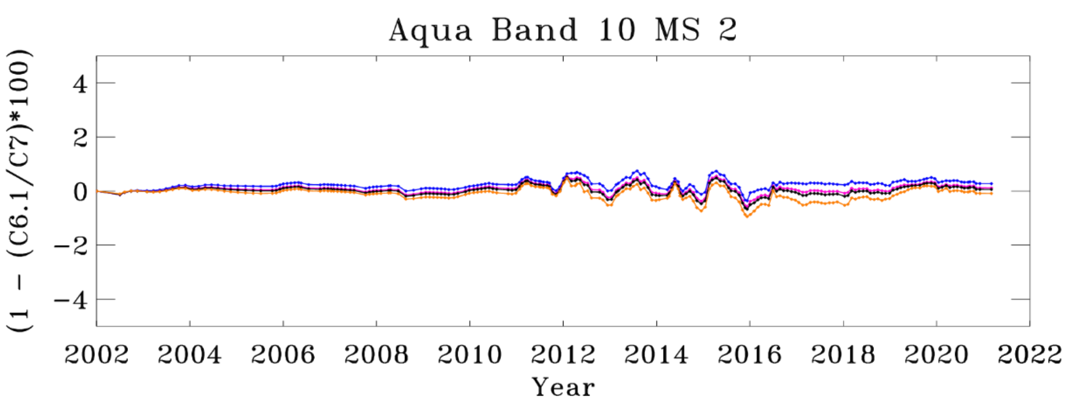
Aqua Band 10 MS 2
(1 − (C6.1/C7)*100)
4
2
0
−2
−4
2002
2004
2006
2008
2010
2012
2014
2016
2018
2020
2022
Year

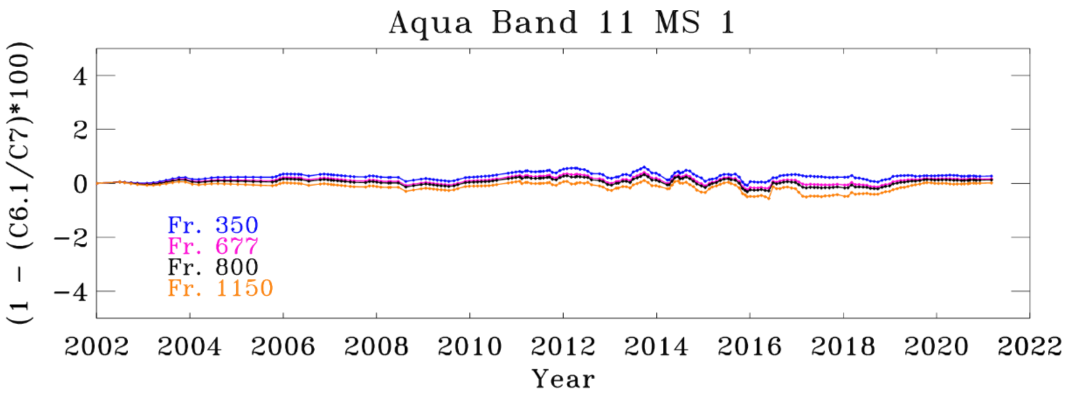
Aqua Band 11 MS 1
(1 − (C6.1/C7)*100)
Year
Fr. 350
Fr. 677
Fr. 800
Fr. 1150

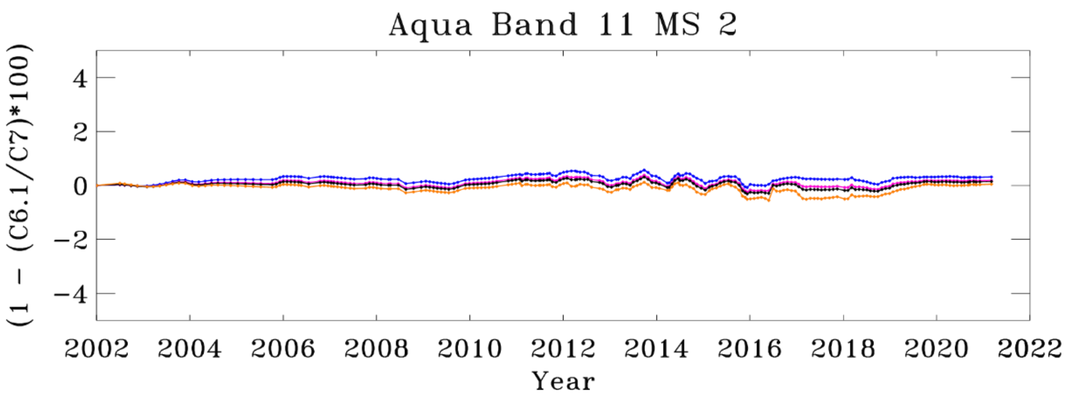
Aqua Band 11 MS 2
(1 − (C6.1/C7)*100)
Year

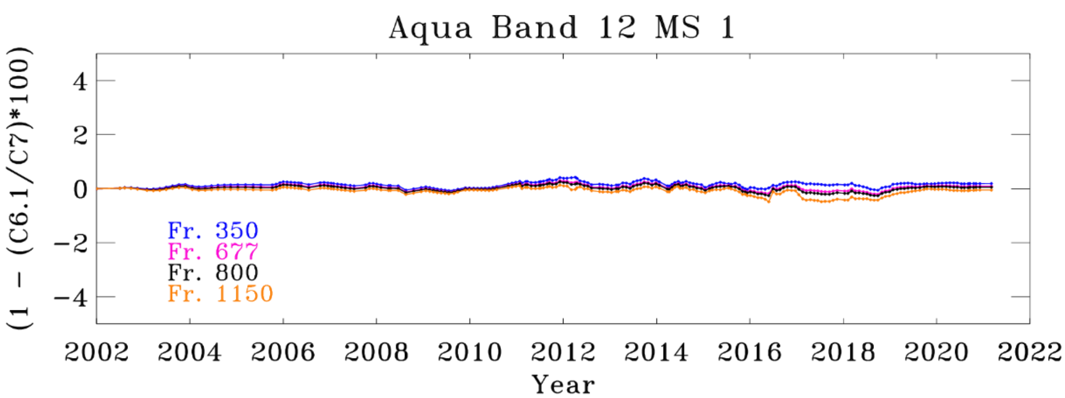
Aqua Band 12 MS 1
(1 − (C6.1/C7)*100)
Year
Fr. 350
Fr. 677
Fr. 800
Fr. 1150

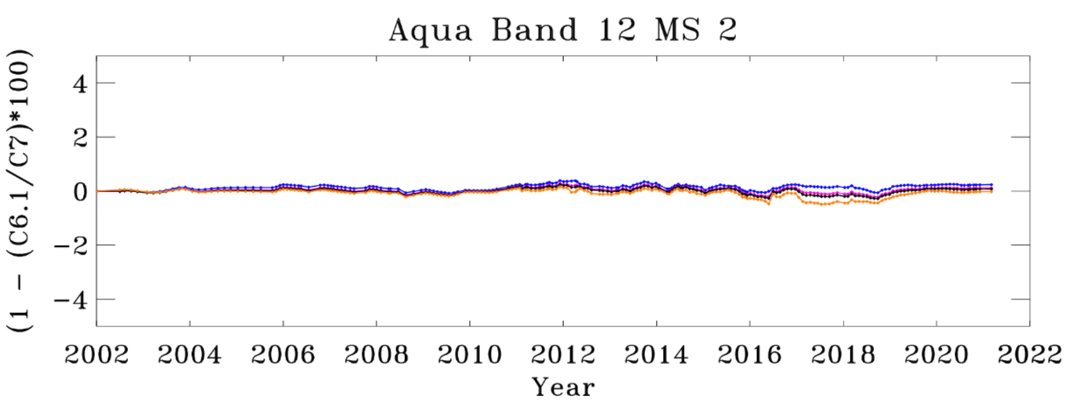
Aqua Band 12 MS 2
(1 − (C6.1/C7)*100)
Year

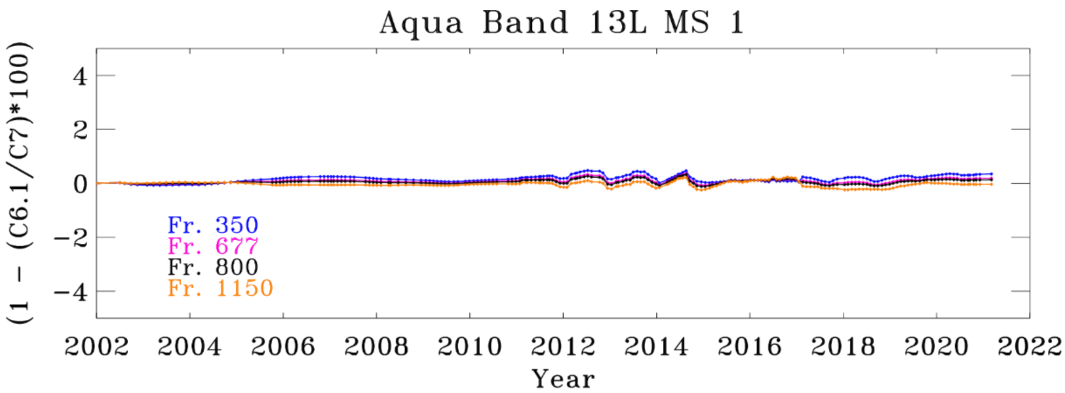
Aqua Band 13L MS 1
(1 − (C6.1/C7)*100)
4
2
0
−2
−4
Fr. 350
Fr. 677
Fr. 800
Fr. 1150
2002 2004 2006 2008 2010 2012 2014 2016 2018 2020 2022
Year

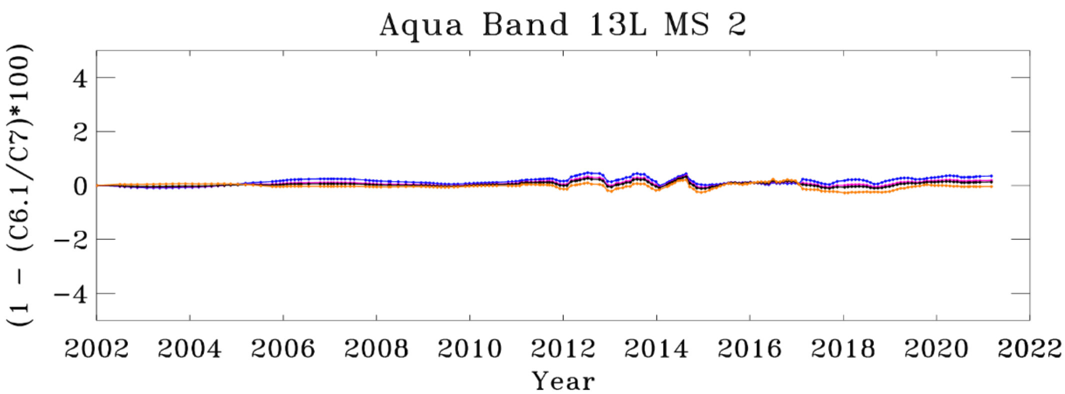
Aqua Band 13L MS 2
(1 − (C6.1/C7)*100)
4
2
0
−2
−4
2002 2004 2006 2008 2010 2012 2014 2016 2018 2020 2022
Year

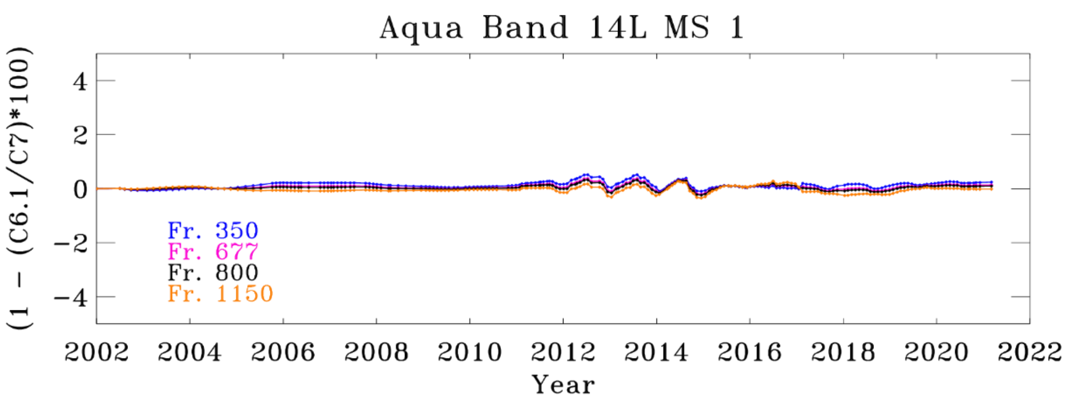
Aqua Band 14L MS 1
(1 − (C6.1/C7)*100)
4
2
0
−2
−4
Fr. 350
Fr. 677
Fr. 800
Fr. 1150
2002 2004 2006 2008 2010 2012 2014 2016 2018 2020 2022
Year

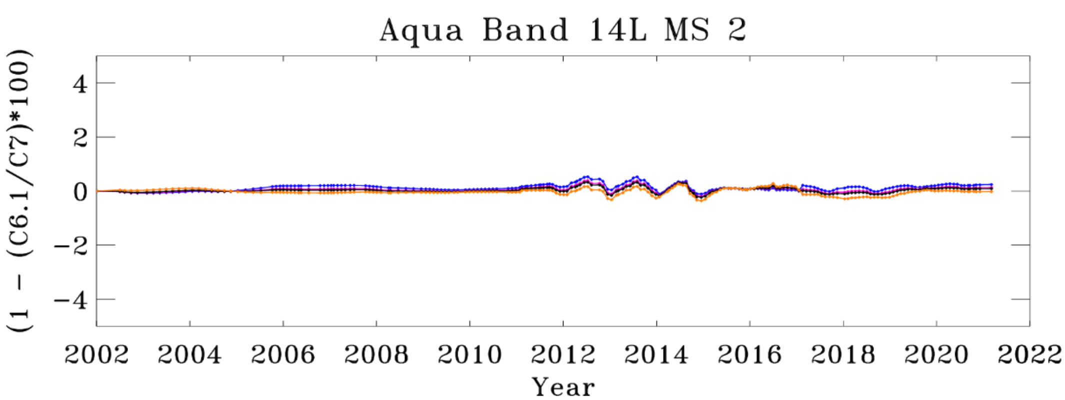
Aqua Band 14L MS 2
(1 − (C6.1/C7)*100)
4
2
0
−2
−4
2002 2004 2006 2008 2010 2012 2014 2016 2018 2020 2022
Year

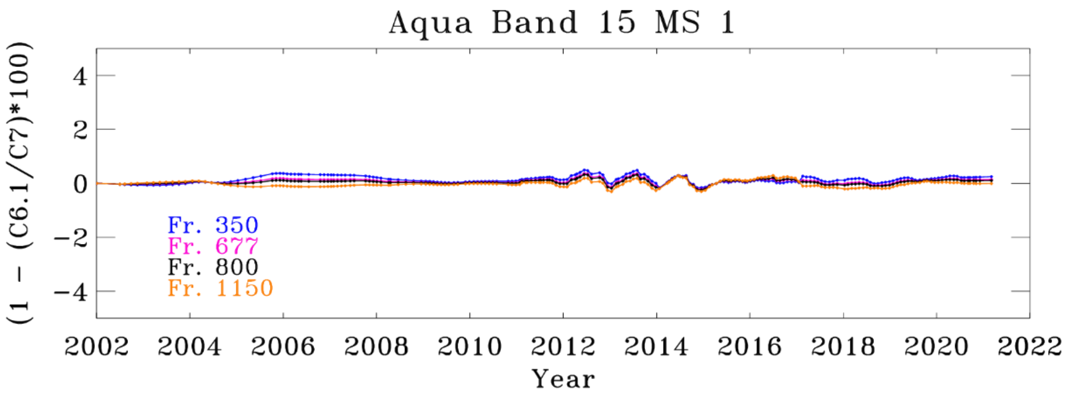
Aqua Band 15 MS 1
(1 − (C6.1/C7)*100)
Year
Fr. 350
Fr. 677
Fr. 800
Fr. 1150

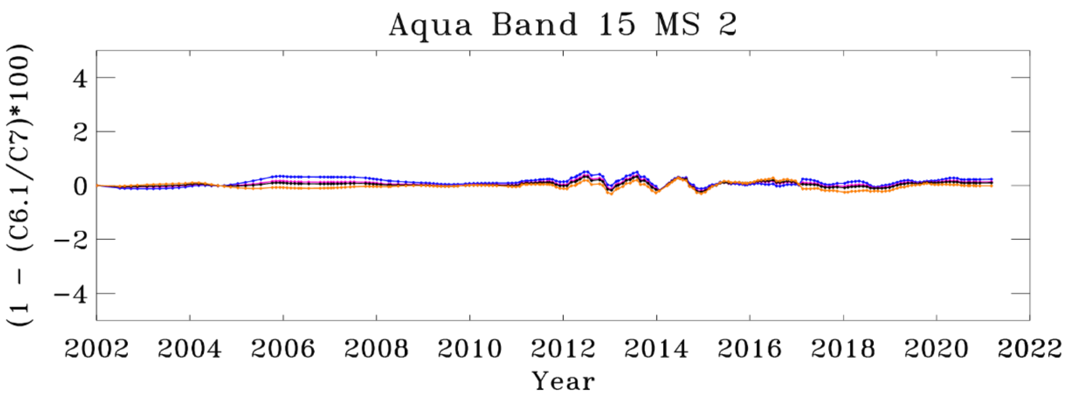
Aqua Band 15 MS 2
(1 − (C6.1/C7)*100)
Year

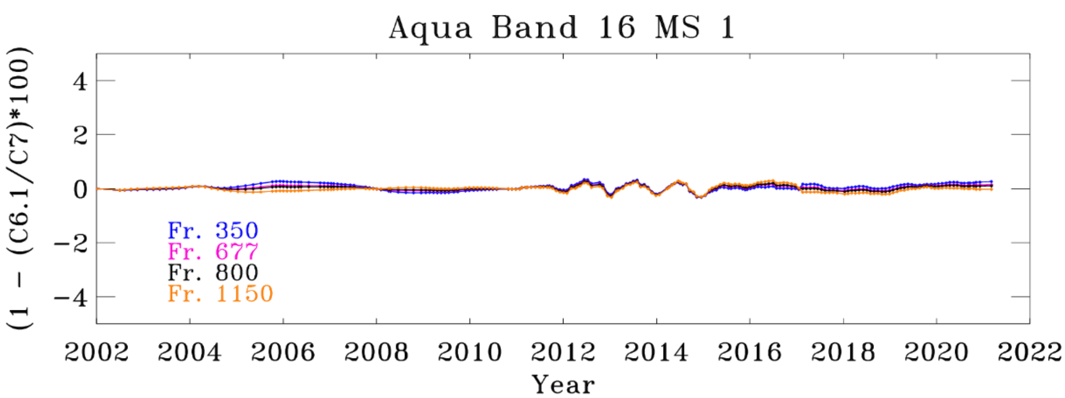
Aqua Band 16 MS 1
(1 − (C6.1/C7)*100)
Year
Fr. 350
Fr. 677
Fr. 800
Fr. 1150

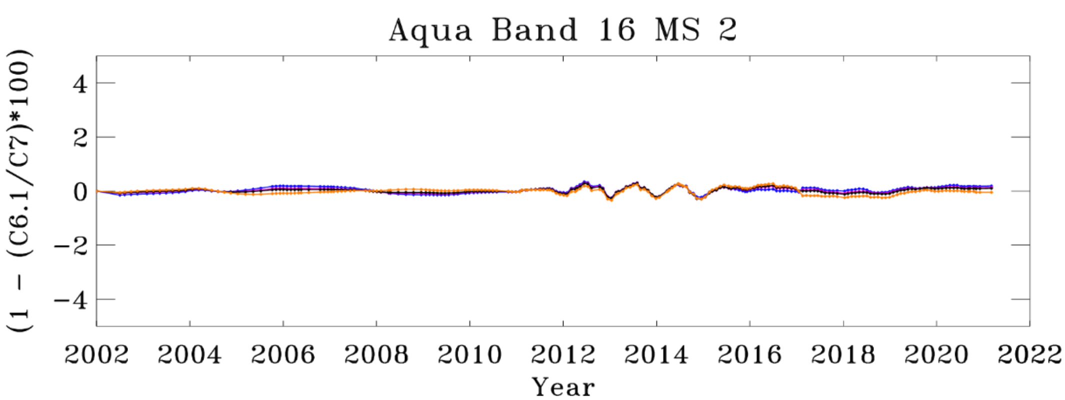
Aqua Band 16 MS 2
(1 − (C6.1/C7)*100)
Year

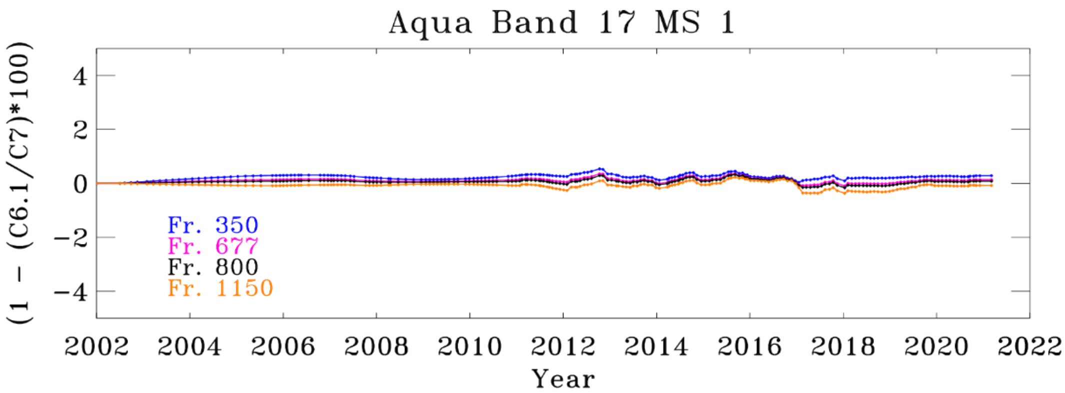

Aqua Band 17 MS 1
(1 − (C6.1/C7)*100)
4
2
0
−2
−4
Fr. 350
Fr. 677
Fr. 800
Fr. 1150
2002
2004
2006
2008
2010
2012
2014
2016
2018
2020
2022
Year

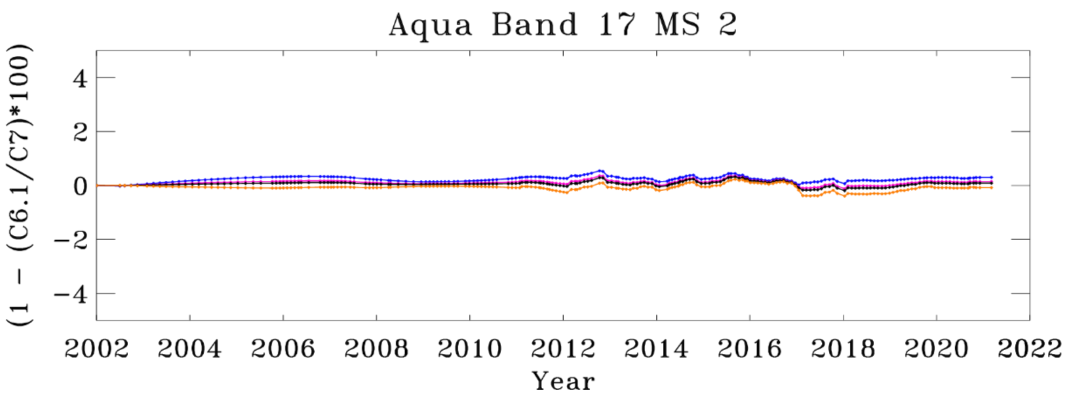

Aqua Band 17 MS 2
(1 − (C6.1/C7)*100)
4
2
0
−2
−4
2002
2004
2006
2008
2010
2012
2014
2016
2018
2020
2022
Year

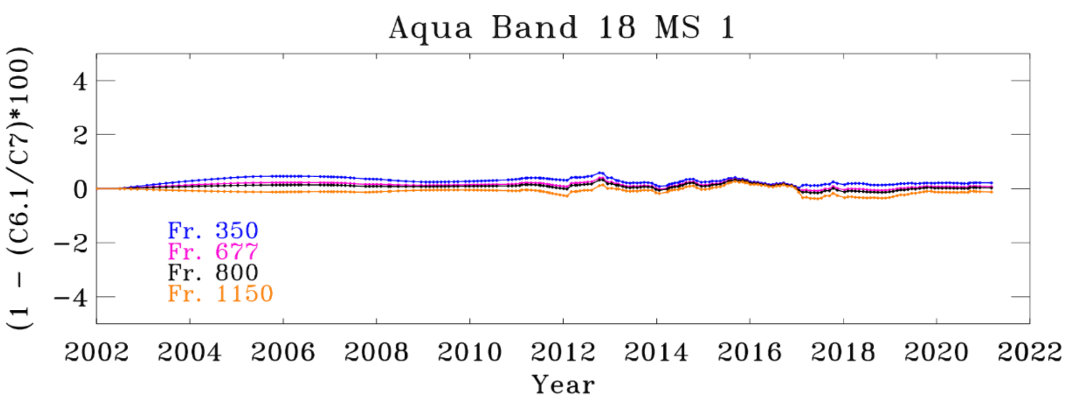

Aqua Band 18 MS 1
(1 − (C6.1/C7)*100)
4
2
0
−2
−4
Fr. 350
Fr. 677
Fr. 800
Fr. 1150
2002
2004
2006
2008
2010
2012
2014
2016
2018
2020
2022
Year

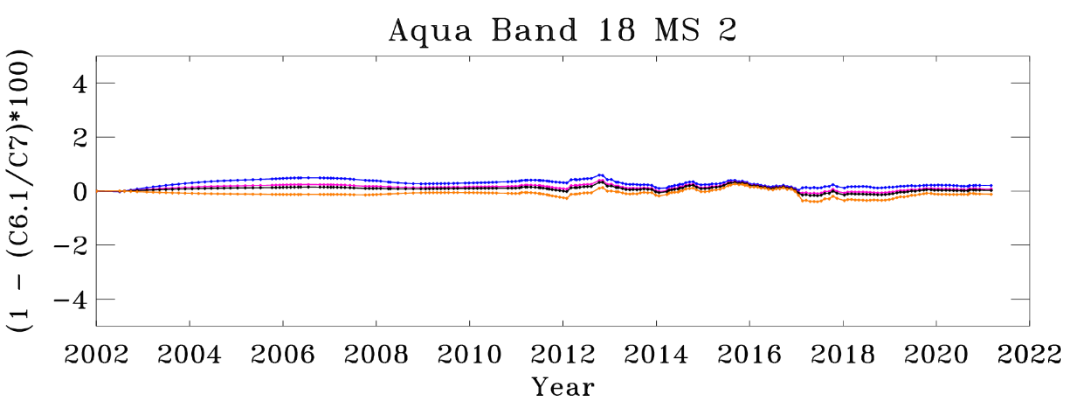

Aqua Band 18 MS 2
(1 − (C6.1/C7)*100)
4
2
0
−2
−4
2002
2004
2006
2008
2010
2012
2014
2016
2018
2020
2022
Year

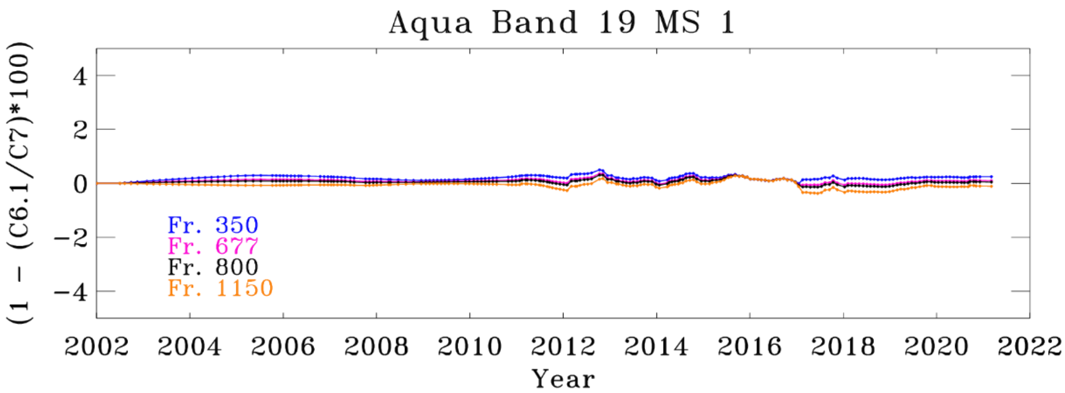
Aqua Band 19 MS 1
(1 − (C6.1/C7)*100)
4
2
0
−2
−4
Fr. 350
Fr. 677
Fr. 800
Fr. 1150
2002 2004 2006 2008 2010 2012 2014 2016 2018 2020 2022
Year

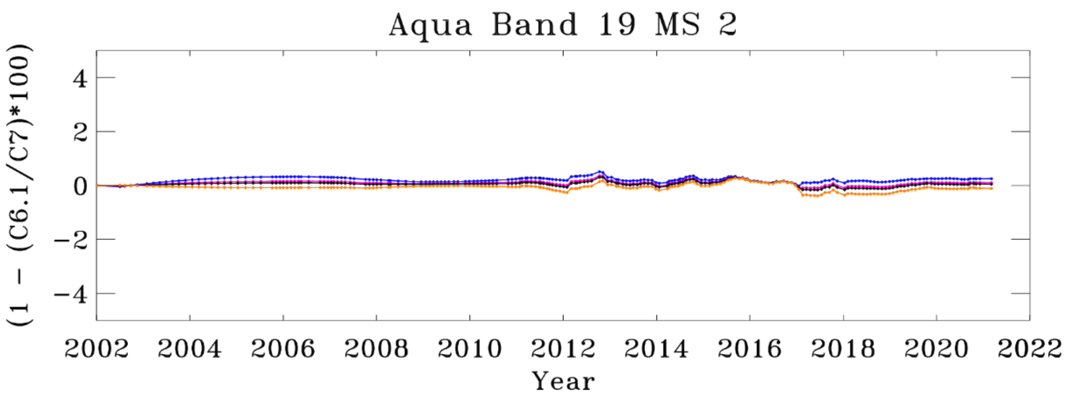
Aqua Band 19 MS 2
(1 − (C6.1/C7)*100)
4
2
0
−2
−4
2002 2004 2006 2008 2010 2012 2014 2016 2018 2020 2022
Year

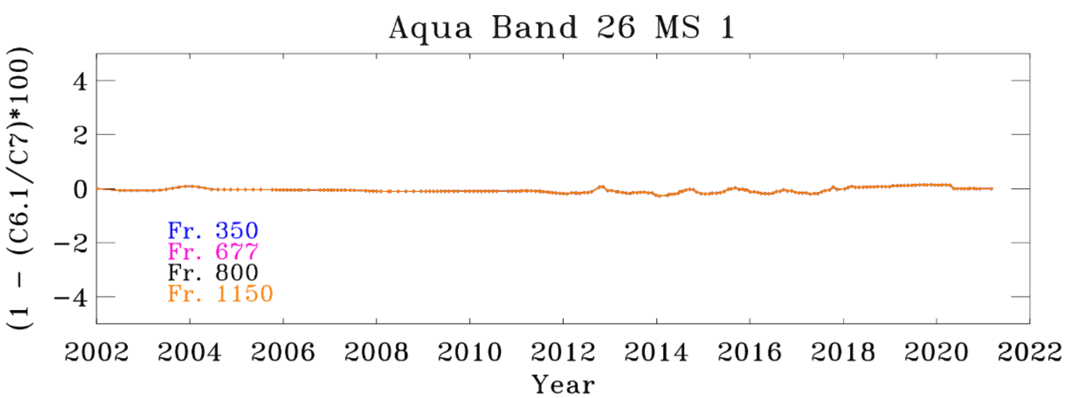
Aqua Band 26 MS 1
(1 − (C6.1/C7)*100)
4
2
0
−2
−4
Fr. 350
Fr. 677
Fr. 800
Fr. 1150
2002 2004 2006 2008 2010 2012 2014 2016 2018 2020 2022
Year

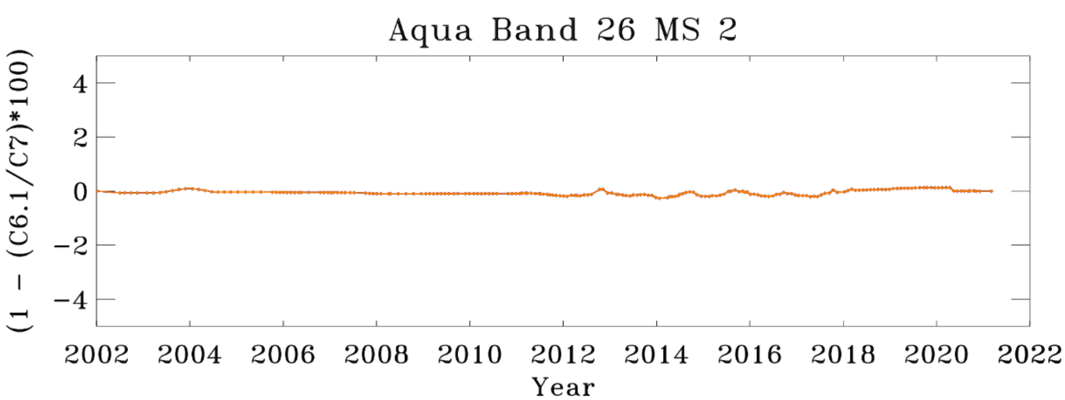
Aqua Band 26 MS 2
(1 − (C6.1/C7)*100)
4
2
0
−2
−4
2002 2004 2006 2008 2010 2012 2014 2016 2018 2020 2022
Year